The derlin Dfm1 promotes retrotranslocation of folded protein domains from the endoplasmic reticulum

Daniel Fonseca and Pedro Carvalho

Sir William Dunn School of Pathology, University of Oxford, South Parks Road, Oxford OX1 3RE, UK

Correspondence should be sent to:

Pedro Carvalho (pedro.carvalho@path.ox.ac.uk); phone: +44 1865 618 654

Abstract

Endoplasmic reticulum (ER) proteins are degraded by proteasomes in the cytosol through ER-associated degradation (ERAD). This process involves retrotranslocation of substrates across the ER membrane, their ubiquitination and subsequent membrane extraction by the Cdc48/Npl4/Ufd1 ATPase complex prior delivery to proteasomes for degradation. Recently a mechanism for the retrotranslocation of misfolded substrates by the Hrd1 ubiquitin ligase complex. However, how substrates folded luminal domains are retrotranslocated remains unknown. Here, we identify Dfm1 as an essential membrane component for the retrotranslocation of proteins with a folded luminal domain. Both Dfm1 intramembrane rhomboid-like motif and the cytosolic Cdc48-binding domain are essential for substrate retrotranslocation. Substrate processing by Dfm1 and the Cdc48 complex requires the ubiquitin shuttle factors Rad23/Dsk2 and the multi-ubiquitination enzyme Ufd2. Our findings suggest a pathway in which a series of ubiquitin modifying factors recruit Dfm1 to resolve a stalled retrotranslocation intermediate due to the presence of a folded luminal domain.

36 **INTRODUCTION**

37 Proteins in the endoplasmic reticulum (ER) are degraded by ER-
38 associated protein degradation (ERAD) (Christianson and Ye, 2014;
39 Ruggiano et al., 2014). This process targets a broad range of substrates,
40 including misfolded membrane and secretory proteins generated as
41 byproducts of biosynthetic processes, as well as a set of folded ER
42 proteins, mostly rate-limiting enzymes of lipid metabolism as part of
43 homeostatic regulatory mechanisms. Thus, ERAD controls both protein
44 and lipid homeostasis in the ER and has a central role in cellular
45 physiology in health and disease (Bhattacharya and Qi, 2019; Needham
46 et al., 2019).

47 ERAD is carried out by multiple, membrane integral ubiquitin ligase
48 complexes, each with specificity for distinct substrate classes
49 (Christianson and Ye, 2014; Ruggiano et al., 2014). In yeast, there are
50 three ERAD ubiquitin ligase complexes -the Hrd1, Doa10 and Asi
51 complexes- and despite their different substrate specificities, the
52 general steps leading to substrate degradation are similar (Wu and
53 Rapoport, 2018). Upon recognition and engagement with an ERAD
54 ubiquitin ligase complex, substrates are transported across the ER
55 membrane into the cytosol, a process called retrotranslocation. Once
56 exposed on the cytosolic surface of the ER, substrates are

polyubiquitinated and subsequently extracted from the ER membrane through the activity of the Cdc48 complex, which includes the hexameric Cdc48 ATPase as well as Npl4 and Ufd1 cofactors (Bays et al., 2001; Ye et al., 2001; Jarosch et al., 2002; Stein et al., 2014; Bodnar and Rapoport, 2017). A number of adaptor proteins, including the multi-ubiquitination enzyme Ufd2 and the shuttle factors Rad23 and Dsk2, finally hand the ubiquitinated substrate to the proteasome for degradation (Medicherla et al., 2004; Richly et al., 2005; Baek et al., 2011).

Despite this general scheme, the molecular mechanisms of the individual ERAD steps are less clear, in particular substrate retrotranslocation across the ER membrane. *In vivo* and *in vitro* studies suggest that for ER luminal substrates, the major retrotranslocation component is the Hrd1 ubiquitin ligase (Carvalho et al., 2010; Baldridge and Rapoport, 2016; Schoebel et al., 2017; Vasic et al., 2020; Wu et al., 2020). Hrd1-mediated retrotranslocation depends on its membrane domain, which recent cryo-EM studies revealed to display features reminiscent of other protein-conducting channels such as the Sec translocon that transports unfolded, newly synthesized proteins into the ER lumen (Schoebel et al., 2017; Wu et al., 2020). The yeast derlins Der1 and Dfm1, members of the rhomboid protein superfamily

78 (Freeman, 2014), have also been implicated in retrotranslocation
79 (Mehnert et al., 2014; Neal et al., 2018; Wu et al., 2020). Despite their
80 similarity, Der1 and Dfm1 appeared to have distinct substrate
81 specificity. While Der1 interacts with and is required for the
82 degradation of misfolded ER luminal substrates (Knop et al., 1996;
83 Carvalho et al., 2006; Denic et al., 2006), Dfm1 appears to target mostly
84 misfolded membrane proteins (Stolz et al., 2010; Neal et al., 2018). The
85 basis for these substrate preferences as well as the precise
86 mechanisms by which ERAD components facilitate retrotranslocation
87 remain obscure. The picture is even less clear for the
88 retrotranslocation of ERAD substrates containing folded domains. It is
89 well established that folded domains within the ER lumen slow down
90 the degradation of ERAD substrates suggesting that their
91 retrotranslocation is challenging (Tirosh et al., 2003; Bhamidipati et al.,
92 2005; Carvalho et al., 2010; Shi et al., 2019). However, how such
93 domains are retrotranslocated and whether the process requires
94 additional components is unknown.

95 Most ERAD substrates characterized so far are degraded constitutively
96 and exist in cells as an heterogeneous ensemble of intermediates.
97 Constitutive degradation of substrates also precludes the uncoupling
98 between protein folding and retrotranslocation. Here, we

99 circumvented these problems by employing an inducible auxin-based
100 degron system to study protein retrotranslocation. By uncoupling
101 protein folding from subsequent steps, we searched for factors
102 required for the retrotranslocation of luminal folded domains. We
103 uncovered that the retrotranslocation of folded domains requires
104 specifically the derlin Dfm1, while ERAD components necessary for the
105 retrotranslocation of misfolded proteins, such as Hrd1 or Der1 are
106 dispensable. Dfm1 function requires both its rhomboid-like membrane
107 domain as well as its cytosolic interaction with the Cdc48/Npl4/Ufd1
108 ATPase complex. Finally, we show that a cascade of ubiquitin
109 processing factors is necessary for retrotranslocation mediated by
110 Dfm1 and the Cdc48 complex. These findings delineate a pathway for
111 the resolution of halted retrotranslocation events due to the presence
112 of folded luminal domains.

113

114

115 **RESULTS**

116 **An auxin-induced assay to study membrane protein**
117 **retrotranslocation**

118 To study how folded luminal domains in membrane proteins are
119 retrotranslocated for proteasomal degradation we generated a
120 chimeric membrane protein with the tightly folded dihydrofolate
121 reductase (DHFR) domain from *E. coli* in the ER lumen. Generation of
122 DHFR fusion proteins is a well-established approach to study protein
123 translocation across lipid bilayers (Eilers and Schatz, 1986; Arkowitz
124 et al., 1993; Gambill et al., 1993; Tirosh et al., 2003; Bhamidipati et al.,
125 2005; Shi et al., 2019). The chimeric membrane protein was
126 engineered to adopt a type I topology in the ER membrane with the N-
127 terminal signal sequence of the ER chaperone Kar2 followed by a triple
128 HA tag, an opsin glycosylation site, the DHFR domain and the
129 transmembrane segment of Ost1, an ER protein. The cytosolic domain
130 of the chimera contained four tandem repeats of the 44-amino acid
131 minimal degron (AID*) derived from the *Arabidopsis thaliana* IAA17
132 protein (Morawska and Ulrich, 2013) followed by nine repeats of the
133 MYC epitope. The chimeric construct was termed inducible Retro-
134 Clogger (iRC) for reasons explained below (Figure 1A).

135 Using fractionation experiments, we established that the iRC substrate
136 was inserted in the ER membrane (Figure 1B). To confirm that iRC
137 acquired the correct topology we examined whether iRC the opsin
138 sequence was glycosylated. Treatment of yeast lysates with Peptide:N-
139 glycosidase F (PNGaseF), which digest the N-glycans, resulted in faster
140 iRC migration by SDS-PAGE (Figure 1C). Thus, iRC is targeted to the ER
141 membrane with its N-terminus facing the ER lumen (Figure 1D).

142 ER ubiquitin ligases, such as Hrd1, are required for both ubiquitination
143 and retrotranslocation of ERAD substrates (Carvalho et al., 2010; Stein
144 et al., 2014; Baldridge and Rapoport, 2016; Vasic et al., 2020). To study
145 substrate retrotranslocation bypassing the need of ubiquitination by
146 the endogenous ER-resident ubiquitin ligases, we exploited the plant-
147 based auxin-induced degradation (AID) (Nishimura et al., 2009;
148 Morawska and Ulrich, 2013). The AID system relies on the expression
149 of a plant-specific F-box protein, Tir1, to recognize AID* motifs in
150 substrates only in the presence of auxin (indole-3-acetic acid, or IAA),
151 triggering their polyubiquitination and degradation (Figure 1D).

152 In yeast cells expressing constitutively the *Arabidopsis thaliana* Tir1
153 (AtTir1) and in the absence of auxin, iRC is a long-lived protein. Even
154 upon inhibition of protein synthesis with cycloheximide, there is no
155 appreciable iRC turnover over a period of 60 minutes (Figure 1E). This

156 was not due to ineffective translation inhibition as Tir1 protein levels
157 decrease over time, indicating that it is a short-lived protein. Upon
158 auxin addition, the iRC was rapidly degraded irrespective of the
159 presence of cycloheximide (without cycloheximide $t_{1/2}$=15min; with
160 cycloheximide $t_{1/2}$=10min). Importantly, iRC degradation was selective
161 even at higher auxin concentrations (Figures 1E and F). Thus, auxin-
162 induced ubiquitination of iRC is sufficient to trigger its
163 retrotranslocation and degradation in an acute and synchronous
164 manner.

165 Long exposures of the blots with the iRC chases upon auxin addition
166 revealed two interesting features (Figure 1E). First, auxin addition
167 resulted in high molecular weight smears suggestive of iRC
168 ubiquitination. Second, while most iRC was degraded, auxin addition
169 resulted in the appearance of small amounts of ~40kDa fragments.
170 These fragments did not contain the MYC epitope present at the C-
171 terminal region of full-length iRC (see below). Thus, based on the size,
172 they likely correspond to the tightly folded DHFR, suggesting that
173 retrotranslocation of this domain is rate-limiting.

174

175 **iRC degradation does not require ERAD ubiquitin ligases**

176 Increasing evidence implicates the ERAD ubiquitin ligases in substrate
177 retrotranslocation (Carvalho et al., 2010; Stein et al., 2014; Baldridge
178 and Rapoport, 2016; Natarajan et al., 2020; Wu et al., 2020).
179 Therefore, we tested whether they were necessary for iRC
180 retrotranslocation and degradation. Individual deletion of Asi1, Hrd1
181 and Doa10 did not prevent auxin-induced degradation of iRC (Figure
182 2A). Moreover, the degradation of iRC was unaffected by simultaneous
183 deletion of the three ubiquitin ligases or the ubiquitin-conjugating
184 enzyme Ubc7 involved in all ERAD branches (Figure 2A). As in *wild-*
185 *type* (*WT*) cells, induction of iRC degradation in ERAD ubiquitin ligase
186 mutants resulted in minute accumulation of the ~40kDa fragment.
187 These results indicate that auxin-induced degradation of iRC substrate
188 is independent of the canonical ERAD ubiquitin ligases and does not
189 require their retrotranslocation activity.

190

191 **iRC DHFR domain accumulates in Dfm1 mutant cells**

192 Derlins are small multi-pass ER membrane proteins implicated in the
193 degradation of luminal (Knop et al., 1996; Lilley and Ploegh, 2004; Ye
194 et al., 2004; Oda et al., 2006) and membrane (Lilley and Ploegh, 2004;
195 Ye et al., 2004; Stolz et al., 2010; Neal et al., 2018) ERAD substrates.
196 They share similarity with rhomboid intramembrane proteases but

197 lack the catalytic activity (Greenblatt et al., 2011) and there are
198 suggestions that they may be involved in retrotranslocation (Lilley and
199 Ploegh, 2004; Ye et al., 2004; Mehnert et al., 2014; Neal et al., 2018; Wu
200 et al., 2020). We tested the role of the yeast derlins Der1 and Dfm1 in
201 iRC retrotranslocation and degradation. In the absence of Der1, Dfm1
202 or both, the degradation kinetics of full-length iRC appeared unaffected
203 (Figure 2B). Simultaneous deletion of Der1 or Dfm1 with all ERAD
204 ubiquitin ligases also did not affect turnover of full-length iRC.
205 Strikingly, in all cells lacking Dfm1, auxin-dependent degradation of
206 iRC resulted in the prominent accumulation of a 37kDa fragment. This
207 fragment was smaller than the one described earlier and appeared in
208 much higher amounts (Figure 2B, compare # and *). In contrast with
209 other reports (Neal et al., 2018), this phenotype of *dfm1Δ* was very
210 stable and was not suppressed over time, even after high number of
211 cells divisions.

212 To determine the identity of the fragments generated in *WT* and *dfm1Δ*
213 cells, they were immunoprecipitated and analyzed by mass
214 spectrometry. Both the ~40 and 37kDa fragments, hereafter called L
215 (long) and S (short) fragments respectively, contain the luminal
216 domains and transmembrane segment of the iRC, varying solely in the
217 size of their cytosolic tails (Figure 2C). While the S fragment contained

218 16 cytosolic residues adjacent to the TMD, the L fragment included an
219 additional portion of the AID* tag (Figure 2C and Figure S1). Together,
220 these data show that Dfm1 plays a unique and essential role in the
221 degradation of iRC luminal domain containing DHFR.

222 Next, we asked whether the accumulation of the S fragment was a
223 direct consequence of the tight folding of DHFR. To this end, we took
224 advantage of DHFR(Pro), a mutant DHFR (Ala29Pro, Trp30Pro,
225 Phe31Pro) which has impaired folding stability (Bhamidipati et al.,
226 2005). An iRC derivative with mutant DHFR(Pro), iRC(Pro), was still
227 degraded in an auxin-dependent manner and with comparable kinetics
228 to original iRC both in *WT* and *dfm1Δ* cells. However, in *dfm1Δ* cells
229 iRC(Pro) was degraded entirely, without accumulation of the S
230 fragment suggesting that Dfm1 requirement increases for substrates
231 with a tightly folded domain in the ER lumen (Figure 2D).

232

233 **Retrotranslocation of a tightly folded domain requires Dfm1**

234 Next, we investigated the nature of the defect in *dfm1Δ* cells leading to
235 accumulation of the S fragment. Fractionation experiments showed
236 that both L and S fragments, generated in *WT* and *dfm1Δ* cells
237 respectively, partition with cellular membranes (Figure 3A). This is

238 consistent with the presence of iRC transmembrane segment in both
239 fragments.

240 To examine the topology of iRC fragments in relation to the ER
241 membrane we first analyzed their glycosylation status by treatment
242 with the Peptide:N-glycosidase F (PNGase F) enzyme. To generate iRC
243 fragments, *WT* and *dfm1Δ* cells were incubated with auxin for 10
244 minutes. Subsequently, whole cell lysates from these cells were treated
245 with PNGase F and analyzed by SDS-PAGE and western blotting. In *WT*
246 and *dfm1Δ* cells, PNGase F treatment resulted in faster migration of
247 full-length iRC, as expected (Figure 3B). Similarly, PNGase F digestion
248 of *WT* extracts resulted in faster migration of the L fragment indicating
249 that the N-terminal glycan was in the lumen of the ER, protected from
250 cytosolic peptide N-glycanase. In contrast, PNGase F treatment of
251 extracts from *dfm1Δ* cells did not affect the mobility of the S fragment
252 suggesting that the N-glycan proximal to the N-terminus had been
253 exposed to and processed by endogenous peptide N-glycanase in the
254 cytoplasm (Figure 3B).

255 To independently validate the topology of auxin-induced L and S
256 fragments, we performed protease protection assays. In the absence of
257 auxin, proteinase-K treatment of microsomes prepared from *WT* and
258 *dfm1Δ* cells showed a similar profile, resulting in a protected fragment

259 of almost 40kDa corresponding to iRC luminal domain (Figure 3C).
260 This data suggest that biogenesis iRC is unaffected in *dfm1Δ* mutant
261 and like in *WT* cells, it has the N-terminus in the ER lumen. A protected
262 fragment of the same size was obtained upon proteinase-K treatment
263 of microsomes prepared from *WT* cells incubated with auxin for 40
264 minutes. In contrast, proteinase-K treatment of microsomes prepared
265 from *dfm1Δ* cells upon 40-minute auxin incubation did not
266 immunoreact with anti-HA antibodies indicating proteinase-K
267 digestion of the HA epitope at the iRC N-terminus (Figure 3C).
268 Altogether, these data show that in *dfm1Δ* mutants the N-terminus of
269 the S fragment encompassing the HA tag and the N-linked glycan is
270 exposed to the cytosolic leaflet of the ER membrane.

271 Protease protection and PNGase F assays in WT cells and the
272 experiments with iRC(Pro) suggest that retrotranslocation of tightly
273 folded DHFR challenges efficient iRC degradation. On the other hand,
274 the protease protection and PNGase F results indicate that the N-
275 terminus of iRC adjacent of DHFR accesses the cytosol in *dfm1Δ* cells.

276 To reconcile these observations and more directly ascertain if the
277 DHFR domain of iRC is effectively retrotranslocated we employed a
278 PEGylation assay with a membrane-impermeable cysteine-reactive
279 reagent, maleimide polyethylene-glycol (mPEG). The iRC-derived

280 fragments generated upon auxin-triggered degradation contain two
281 cysteine residues, both within the DHFR domain. Yeast microsomes
282 prepared from auxin-treated WT and *dfm1Δ* cells were incubated with
283 mPEG in the presence or absence of detergent. After quenching, the
284 samples were immunoprecipitated with an anti-HA antibody and the
285 eluates analyzed by SDS-PAGE and western blotting. In absence of
286 detergent, the fragments remained largely unmodified by mPEG, both
287 in WT and *dfm1Δ* microsomes (Figure 3D). Dissolution of the
288 microsomal membrane with the detergent Triton X-100 resulted in
289 slower migration of the fragments consistent with PEGylation of one of
290 the cysteines (Figure 3D, 1xPEG). This result suggests that the second
291 cysteine is inaccessible to mPEG likely due to sterical constrains in
292 folded DHFR. Indeed, prominent modification of the second cysteine
293 residue was observed in buffer containing 1% SDS, a condition
294 inducing DHFR unfolding (Figure 3D, 2xPEG). These results were
295 confirmed by PEGylation experiments in cells expressing iRC-
296 derivatives with mutations in the two cysteine residues within DHFR
297 (C191A and C258A) (Figure 3D). Together, these experiments show
298 that iRC fragments are in the lumen of the ER. Moreover, the strong
299 accumulation of DHFR in the ER lumen (in the form of S fragment) in
300 the *dfm1Δ* mutant reflects a defect of these cells in the

301 retrotranslocation of tightly folded domains. Of note, the S fragment
302 accumulated in *dfm1Δ* cells displays a unique topological orientation,
303 with its N-terminus facing the cytosol (Figure 3E).

304

305 **Distinct Dfm1 domains involved in the retrotranslocation of a**
306 **tightly folded domain**

307 Dfm1 consists of a rhomboid-like membrane domain followed by an
308 extended cytosolic C-terminus encompassing two SHP boxes shown to
309 bind to Cdc48 (Sato and Hampton, 2006; Greenblatt et al., 2011).
310 Rhomboid-like signature motifs include the WR residues in a luminal
311 loop and the GxxxG sequence in the sixth transmembrane segment
312 (Lemberg and Freeman, 2007). Both WR and GxxxG motifs are
313 required for the function of rhomboid proteases as well as catalytically
314 inactive derlins, such as Dfm1 (Lemberg et al., 2005; Greenblatt et al.,
315 2011; Neal et al., 2018). To test the contribution of Dfm1 rhomboid-
316 like domain in DHFR retrotranslocation we overexpressed the mutants
317 Dfm1$^{(WR\text{-}AA)}$ or Dfm1$^{(GxxxG\text{-}AA)}$ in *dfm1Δ* cells. While overexpression of
318 Dfm1 prevented accumulation of iRC S fragment, this fragment was
319 still present in cells expressing comparable levels of Dfm1$^{(WR\text{-}AA)}$ or
320 Dfm1$^{(GxxxG\text{-}AA)}$ (Figure 4A). Curiously, overexpression of Dfm1$^{(WR\text{-}AA)}$ in
321 *WT* cells also led to S fragment accumulation indicating a dominant-

322 negative function of this mutation (Figure 4B). Thus, Dfm1 rhomboid-
323 like activity is required for the retrotranslocation and degradation of
324 iRC folded luminal domain.

325 To examine the role of Dfm1 SHP boxes in iRC degradation we
326 generated Dfm1$^{(1-283)}$, a C-terminal truncation that removes both SHP
327 motifs. Dfm1$^{(1-283)}$ did not affect the degradation rate of the full-length
328 iRC however it led to a four-fold increase in the accumulation of L
329 fragment (Figure 4C). These data suggest that Dfm1 rhomboid-like
330 signature motifs and Cdc48-interacting SHP boxes have distinct roles
331 in retrotranslocation of iRC folded domain.

332

333 **Dfm1 and the Cdc48 complex cooperate in the retrotranslocation**
334 **of a luminal folded domain**

335 The cytosolic Cdc48 ATPase, with the co-factors Npl4 and Ufd1, plays a
336 central role in protein retrotranslocation from the ER (Wu and
337 Rapoport, 2018). To test the role of Cdc48 complex in iRC
338 retrotranslocation and degradation, we used a well-characterized
339 temperature-sensitive (ts) allele, *NPL4-1*, which can be inactivated at
340 37°C (Ye et al., 2001; Hitchcock et al., 2003). At this temperature atTir1
341 is non-functional (Nishimura et al., 2009) and the Tir1 from *Oryza*
342 *sativa* (OsTir1) was used instead. While OsTir1 is active at a wider

343 temperature range, its auxin-dependent recognition of iRC is less
344 stringent and basal degradation of iRC is observed even in the absence
345 of auxin (Figure S2). At 25°C, the permissive temperature at which
346 *NPL4-1* retains some residual activity, auxin treatment resulted in iRC
347 degradation with the generation of the expected L and S fragments in
348 cells with and without *DFM1*, respectively (Fig5A, left panel).
349 Inactivation of Npl4 by a temperature shift to 37°C led to an increase in
350 the amount of L fragment in comparison to WT cells (Fig5A, right
351 panel). Importantly, Npl4 inactivation in *dfm1Δ* cells also resulted in a
352 strong accumulation of L fragment with a concomitant decrease in S
353 fragment. Similar results were obtained upon inactivation of Cdc48
354 complex using a different allele, *cdc48-6* (Schuberth and Buchberger,
355 2005; Ruggiano et al., 2016) (Figure 5B). These experiments indicate
356 that Cdc48 complex plays an important role in iRC retrotranslocation
357 and that its function precedes the one of Dfm1.

358

359 To investigate the association of iRC with Dfm1 and the Cdc48 complex
360 we used immunoprecipitation. Cells were treated with auxin to trigger
361 iRC degradation and iRC was immunoprecipitated from detergent-
362 solubilized crude membrane fractions. In WT cells, a small fraction of
363 both Dfm1 and Cdc48 associated with iRC. This association increased

364 in cells expressing Cdc48-6, a substrate-trapping allele, suggesting that
365 the interaction of iRC with these factors is transient (Schuberth and
366 Buchberger, 2005; Ruggiano et al., 2016). In *dfm1Δ* cells, iRC
367 interaction with Cdc48-6 was maintained while its association with *WT*
368 Cdc48 appeared slightly reduced. In all cases, the abundant ER
369 membrane protein Dpm1 did not associate with iRC suggesting that its
370 interactions with Dfm1 and Cdc48 were specific.

371

372 **Cdc48 recruitment to retrotranslocation intermediates requires**
373 **Ufd2 and Rad23/Dsk2**

374 ERAD involves various adaptor proteins which facilitate the interaction
375 of substrates with key effectors such as the Cdc48 ATPase or the
376 proteasome (Jentsch and Rumpf, 2007; Wolf and Stolz, 2012). We
377 wondered whether these adaptors were required for iRC degradation.
378 Among ERAD adaptors are Ubx2, involved in recruiting Cdc48 to the
379 ER membrane (Neuber et al., 2005; Schuberth and Buchberger, 2005),
380 and the redundant substrate shuttling factors Rad23 and Dsk2
381 (Medicherla et al., 2004; Tsuchiya et al., 2017). The degradation of iRC
382 in *ubx2Δ* cells was indistinguishable from WT cells (Figure S3). In
383 contrast, *rad23Δ dsk2Δ* mutant cells showed strongly impaired iRC
384 degradation and even the generation of L fragment was defective

385 (Figure 6A). Strikingly, a similar phenotype was observed in cells
386 lacking Ufd2, a polyubiquitination enzyme shown to bridge Cdc48 to
387 Rad23 and Dsk2 (Richly et al., 2005; Baek et al., 2011) (Figure 6A).
388 These results suggested that Rad23/Dsk2 and Ufd2 were required
389 upstream of Cdc48, perhaps from a defect in Cdc48 recruitment to iRC.
390 To directly test this possibility, we analyzed the interaction of Cdc48
391 with iRC before and after inducing its auxin-dependent ubiquitination.
392 In the absence of auxin no interaction between iRC and Cdc48 was
393 observed, as expected (Figure 6B). However, upon iRC ubiquitination
394 by addition of auxin resulted in its interaction with Cdc48. The
395 interaction was specific as the other abundant complexes with
396 ubiquitin-binding activity, such as the proteasome did not co-
397 precipitate with iRC. Dfm1 stabilizes Cdc48 interaction with iRC, as less
398 Cdc48 co-precipitated with iRC in *dfm1Δ* cells. Remarkably, the
399 interaction between iRC and Cdc48 was lost both in *rad23Δdsk2Δ* and
400 in *ufd2Δ* cells (Figure 6B and Figure S4). Together these experiments
401 indicate that Rad23/Dsk2 shuttle factors, together with Ufd2, facilitate
402 the recruitment of Cdc48 to iRC.

403

404

405

406 **DISCUSSION**

407 Retrotranslocation of folded protein domains is challenging and their
408 presence slows down the degradation of ERAD substrates (Tirosh et
409 al., 2003; Bhamidipati et al., 2005; Shi et al., 2019). However, how
410 proteins with folded luminal domains are retrotranslocated across the
411 ER membrane is unknown. To investigate this issue, we developed the
412 iRC, a conditional substrate whose biogenesis and folding can be
413 uncoupled from its degradation, triggered by auxin.

414 Based on our data, we propose the following model for iRC
415 retrotranslocation and degradation (Figure 7). In the absence of auxin,
416 the iRC is a long-lived ER membrane protein consistent with it being
417 properly folded and not recognized by quality control processes such
418 as ERAD. Auxin-induced iRC ubiquitination results in its conversion
419 into the L fragment as well as in its association with the
420 Cdc48/Npl4/Ufd1 ATPase complex, both requiring the ubiquitin
421 shuttle factors Rad23/Dsk2 and the multiubiquitin chain extension
422 enzyme Ufd2. The proteasome has been implicated in proteolytic
423 clipping of several ubiquitinated ER proteins (Hoppe et al., 2000;
424 Kohlmann et al., 2008) and likely also contributes to the L fragment
425 generation, a possibility should be directly tested in future studies.

426 The role of Rad23/Dsk2 and Ufd2 in Cdc48 complex recruitment
427 should be also further characterized. These factors shuttle
428 ubiquitinated substrates from Cdc48 to the proteasome (Medicherla et
429 al., 2004; Richly et al., 2005; Baek et al., 2011). However, recent studies
430 in human cells demonstrated that RAD23B, the human homolog of
431 Rad23, can also function in concentrating ubiquitinated substrates for
432 subsequent processing by p97, the Cdc48 homolog, and the
433 proteasome (Yasuda et al., 2020). Interestingly, this role of RAD23B
434 was observed specifically during hyperosmotic stress, a condition that
435 like auxin-induced ubiquitination of iRC, leads to an acute increase in
436 ubiquitinated substrates. Dfm1 has also been shown to facilitate Cdc48
437 association with ER membranes. (Neal et al., 2018). Consistently, while
438 Cdc48 can be recruited to iRC in *dfm1Δ* cells, persistent association of
439 Cdc48 with the iRC requires Dfm1, in particular its SHP boxes. Indeed,
440 cells expressing Dfm1(1-283), a truncated Dfm1 lacking the SHP boxes,
441 showed increased accumulation L fragment, just like Cdc48 complex
442 mutants. Thus, Rad23/Dsk2, Ufd2 and Dfm1 all appear to contribute to
443 the stable engagement of Cdc48 complex with iRC. The Cdc48 complex,
444 through rounds of ATP hydrolysis, pulls on iRC domain exposed to the
445 cytoplasm while Dfm1, through its rhomboid-like membrane region,
446 interacts with and facilitates the retrotranslocation of iRC folded

447 luminal domain. The joint activity of Cdc48 complex and Dfm1 results
448 in iRC release from the membrane for subsequent degradation by the
449 proteasome (Figure 7).

450 Dfm1 was necessary for the degradation of iRC while iRC(Pro), an
451 analogous substrate containing a luminal unfolded DHFR domain, was
452 degraded independently of Dfm1. The specific requirement of Dfm1 for
453 substrates with folded luminal domains suggests that it has a role in
454 the resolution of stalled retrotranslocation intermediates. Whether this
455 is achieved by promoting the retrotranslocation of luminal domains in
456 their folded state or by assisting their unfolding prior
457 retrotranslocation is an important open question.

458 In the absence of Dfm1, iRC accumulates in the form of S fragment. This
459 fragment, which is generated in a Cdc48-dependent manner, has an
460 interesting topology, with the N-terminus exposed to the cytoplasm
461 while the folded DHFR domain fails to retrotranslocate and remains
462 within the ER lumen (Figure 3E). Whether S fragment is a general
463 intermediate in iRC degradation or an off-pathway product generated
464 only in the absence of Dfm1 is unclear.

465 Dfm1 rhomboid-like signature motifs are required for the
466 retrotranslocation of folded DHFR domain as observed by the
467 accumulation of S fragment in cells expressing Dfm1 rhomboid-like

468 signature mutants. In a recent cryo-EM structure of the Dfm1 homolog
469 Der1, these rhomboid-like signature motif form a hydrophilic cavity on
470 the luminal side of the ER membrane (Wu et al., 2020). As observed in
471 previous structures of active rhomboid proteases (Wang et al., 2006;
472 Wu et al., 2006; Ben-Shem et al., 2007), the signature motif also leads
473 to thinning of the surrounding membrane. In principle, both the
474 hydrophilic cavity and the ability to thin the membrane may facilitate
475 Dfm1-mediated retrotranslocation.

476 Importantly, expression of Dfm1 rhomboid-like signature motif
477 mutants leads to S fragment accumulation even in cells with *WT* Dfm1.
478 The dominant-negative effect of these mutants suggests that Dfm1
479 functions as an oligomer, as previously shown by immunoprecipitation
480 experiments (Goder et al., 2008; Stolz et al., 2010). Alternatively,
481 mutant Dfm1 may titrate away an essential component for iRC
482 degradation, such as Cdc48 or other currently unknown factors. While
483 this can only be clarified experimentally, it should be mentioned that
484 rhomboid proteases notably function as monomers (Kreutzberger and
485 Urban, 2018). In addition, a cryo-EM structure of the Hrd1 complex
486 required for the retrotranslocation of luminal misfolded proteins
487 contains a single Der1 molecule (Wu et al., 2020).

488 Dfm1 was recently implicated in the retrotranslocation of misfolded
489 membrane proteins (Stolz et al., 2010; Neal et al., 2018). These include
490 substrates of both Doa10- and Hrd1-dependent ERAD, consistent with
491 previous immunoprecipitation studies which showed interactions
492 between Dfm1 and the two ubiquitin ligases (Goder et al., 2008; Stolz
493 et al., 2010). Curiously, the requirement for Dfm1 in retrotranslocation
494 of misfolded membrane proteins is transient. While these substrates
495 are stabilized in freshly generated *dfm1Δ* cells, after a few generations
496 these mutants are capable of degrading misfolded membrane proteins
497 with a kinetics similar to *WT* cells (Neal et al., 2018). The spontaneous
498 and rapid phenotypic suppression in *dfm1Δ* involved the duplication of
499 the *HRD1* locus pointing to redundant roles of Hrd1 and Dfm1 in the
500 degradation of misfolded membrane proteins. In contrast, we observe
501 that the requirement of Dfm1 in the degradation of iRC degradation is
502 stable over time and was independent of *HRD1* as well as other ERAD
503 components. Despite the differences, the retrotranslocation of both
504 misfolded and folded membrane proteins involves rhomboid-like
505 signature motifs of Dfm1 as well as its SHP boxes for Cdc48 interaction.
506 Thus, the degradation of misfolded and folded membrane proteins
507 appear to have common as well as distinct steps, both involving Dfm1.

508 It will be interesting to directly compare the roles of Dfm1 in the
509 retrotranslocation of the two types of substrates.

510 Here, we used a single substrate, the iRC, to delineate a simple pathway
511 for the retrotranslocation of membrane proteins with folded luminal
512 domains. While the iRC will be useful for mechanistic studies, it will be
513 of great interest to identify additional substrates following the same
514 degradation route. Several membrane proteins are targeted for
515 degradation upon ubiquitination by soluble ubiquitin ligases. This
516 group include for example SUN2 (Coyaud et al., 2015) or its yeast
517 homologue Mps3 (Koch et al., 2019), both with large folded domains in
518 the ER lumen. Importantly, in neither case, the membrane components
519 required for the degradation have been identified. Our work indicates
520 that Dfm1 or mammalian Derlins are good candidates to test.

521

522 **METHODS**

523 **Yeast strains and Plasmids**

524 The strains used are isogenic either to BY4741 (MATa *ura3Δ0 his3Δ1*
525 *leu2Δ0 met15Δ0*) or FY251 (*MATa ura3-52 his3Δ200 leu2Δ1 trp1Δ63*)
526 and are listed in the Supplementary Table S1. Tagging of proteins and
527 individual gene deletions were performed by standard PCR-based
528 homologous recombination (Longtine et al., 1998) or CRISPR
529 (Laughery et al., 2015). The Dfm1(1-283-SBP) allele lacking residues
530 (284-341) with SBP-tag was generated by CRISPR-based gene editing
531 as described (Laughery et al., 2015). In brief, a single guide RNA
532 sequence targeting the desired region of Dfm1 was designed using
533 online software (http://wyrickbioinfo2.smb.wsu.edu) and cloned into
534 a pML vector (Addgene) containing the Cas9 endonuclease from
535 Streptococcus pyogenes using restriction ligation. Cas9 plasmid along
536 with a PCR amplified template containing the deletion of AA (284-341)
537 were transformed using standard transformation protocol. Colonies
538 were screened by PCR and sequencing of genomic DNA. Positive clones
539 were grown in rich media (YPD) for 2-3 days to allow the loss of Cas9
540 plasmid.

541 Strains with multiple gene deletions and temperature-sensitive alleles
542 were made by crossing haploid cells of opposite mating types, followed

543 by sporulation and tetrad dissection using standard protocols (Fink
544 and Guthrie, 1991). All cloning procedures were carried out with PCR
545 and Gibson-based assembly or restriction ligation. Dfm1-FLAG
546 construct was generated by genomic amplification of *DFM1* gene and
547 cloned into a pRS425-Gal with a single FLAG tag at the C-terminus.
548 Dfm1 signature motif mutants were generated by sit-directed
549 mutagenesis. Coding sequences from iRC construct and O. sativa *TIR1*
550 were ordered as gene blocks. For all strains, a minimal domain of
551 IAA17 consisting of amino acids 71-114 as described in (Morawska
552 and Ulrich, 2013) was used. Following its verification by sequencing,
553 the iRC and variant constructs were amplified inserted either with a
554 CPY promoter or an ADH promoter into the *HO* locus of all strains of
555 interest. Plasmids used in this study are listed in Supplementary
556 Tables S2.

557

558 **Substrate degradation experiments**

559 Cycloheximide shutoff chases were performed as described previously
560 (Foresti et al., 2014.) Briefly, yeast cells were grown either in rich
561 media (YPD) or synthetic media with 2% glucose in exponential phase
562 (OD_{600} 0.6 - 0.9) at 25°C. Over-expression of Dfm1-FLAG variants was
563 driven from the inducible GAL promoter upon constant growth

564 synthetic media (SC-Leucine) with 4% D-Galatactose to exponential
565 phase at 25°C. 6 ODs of cells were harvested, centrifuged for 2 min at
566 3500rpm and resuspended in the appropriate media at 1 OD/mL. For
567 auxin-dependent degradation experiments, auxin (Indole-3-acetic acid,
568 IAA) was added to the cultures from a stock prepared in DMSO to a
569 final concentration of 400 μM. For experiments using OsTir1, cells
570 were treated with 50 μM of auxin. In experiments with cycloheximide,
571 the drug was used at 250 μg/mL from a stock of 12.5 mg/mL prepared
572 in H_2O. At the specified time points 1 OD of cells was collected and
573 whole-cell lysates were prepared using NaOH extraction - cell pellets
574 were treated with 300 μL of 150 mM NaOH for 10 min on ice, briefly
575 centrifuged and resuspended in 50 μL sample buffer (SB; 100 mM
576 Tris/HCl [pH6.8], 3% SDS, 15% glycerol, 75 mM DTT). Samples were
577 then analyzed by SDS-PAGE (0.4 ODs per sample were loaded)
578 followed by immunoblot with the indicated antibodies. Unless
579 indicated, chases were performed at 25°C. Temperature-sensitive
580 mutants were grown at 25˚C and shifted to 37˚C for 1-2.5 hours prior
581 to the addition of auxin. For the experiments with galactose induction,
582 cells were grown directly at 25°C in SC media supplemented with 4%
583 galactose. Data quantification was performed using Image Studio

584 software (Li-Cor) and graphs were plotted in GraphPad Prism v6.
585 Representative images of three independent experiment are shown.

586

587 **Deglycosylation experiments**

588 Cell lysates obtained by NaOH extraction were diluted 1:1 in water to
589 final concentration of SB (50mM Tris/HCl [pH6.8], 1.5% SDS, 7.5%
590 glycerol, 37.5mM DTT). PNGaseF (0.5 µL, 2500U) of was added to 20
591 µL of lysate and incubated for 15 min at 37°C. Samples were then
592 analyzed by SDS-PAGE followed by immunoblot.

593

594 **Membrane fractionation experiments**

595 Cells fractionation experiments 50 ODs of cells were lysed in LB buffer
596 (50mM Tris/HCl [pH7.4], 200 mM NaCl, 1mM EDTA, 2mM
597 phenylmethylsulfonyl fluoride (PMSF) and protease inhibitor cocktail)
598 by 5-6 x 1 min cycles of bead-beating at 4*C. Lysates were cleared by a
599 10 min centrifugation at 2000 rpm. Crude membrane and soluble
600 fractions were obtained from cleared lysates by centrifugation at
601 45000 rpm (25 min at 4°C), using a TLA 100.3 rotor. The membrane
602 pellet was resuspended in sample buffer (100 mM Tris/HCl [pH6.8],
603 3% SDS, 15% glycerol, 75 mM DTT) and solubilized at 65°C for 10 min.

604

605 **Co-Immunoprecipitation**

606 100 ODs of cells were harvested and lysed as described for membrane
607 fractionation experiments, except that the membrane fraction was
608 solubilized in LB + 1% GDN (glyco-diosgenin) supplemented with 1mM
609 PMSF and protease inhibitor cocktail. After 2 hours, the solubilized
610 membranes were precleared by centrifugation for 15 min at max speed
611 on a table-top centrifuge and the supernatant was incubated overnight
612 with 20 µL of anti-HA magnetic beads (Pierce TM). Beads were washed
613 3 times with LB + 0.02% GDN and bound proteins eluted with SB
614 buffer and analyzed by SDS-PAGE and immunoblotting.

615

616 **Protease protection assay**

617 50 ODs of cells were harvested and lysed as described for membrane
618 fractionation experiments, except that the membrane fraction was
619 resuspended in buffer A (20 mM HEPES [pH7.4], 2 mM magnesium
620 acetate, 150 mM KCl, 200 mM sucrose) that lacked protease inhibitors.
621 Total lysates were incubated with Proteinase K (50 µg/mL) or
622 Proteinase K with 1% Triton X-100 for 30 min on ice. The reaction was
623 stopped by the addition of PMSF (2.5 mM final concentration) for 10

624 min on ice, and after the reaction products were diluted 1:1 in SB and
625 analyzed by SDS–PAGE and immunoblotting.

626 **PEGylation assays**.

627 Cells were grown in YPD until OD of 0.75 and added 0.5 mM auxin for
628 40min. 250 ODs of cells were harvested and treated with 10 mM Tris-
629 HCl [pH10.5], 1 mM DTT for 10min at room temperature. Cells were
630 washed with SP buffer (50 mM Tris/HCl pH 7.5, 100 mM NaCl, 0.3 M
631 Sorbitol, 1 mM EDTA, 1 mM phenylmethylsulphonyl fluoride (PMSF), 2
632 mM benzamidine and cOmplete protease inhibitor cocktail (Roche
633 Diagnostics, Mannheim, Germany)) and incubated with zymolyase 20T
634 for ~20min at 37°C. Spheroplasts were washed, resuspended in 5 mL
635 of SP buffer, and were dounced to generate microsomes. Microsome
636 fraction was centrifugated for 5min at 2000rpm to remove unbroken
637 cells. Microsomal lysate (300 µL) were treated with 2.5 mM of
638 methoxy-polyethylene glycol maleimide (Mal-PEG 5K) for 1h on ice
639 and the reaction was quenched with 25 mM DTT for 30 min. In
640 detergent treated reactions, microsomes were mixed with 1% Triton
641 X-100 or 1% SDS prior to the addition of Mal-PEG in a total volume
642 reaction of 400µL. Samples were diluted to 1.2mL in LB supplemented
643 with 1% Triton X-100 and incubated overnight with 20 µL anti-HA
644 beads (Pierce TM). Beads were washed 3 times with LB + 1% Triton X-

645 100 and bound proteins eluted with 20 μL SB buffer and analyzed by
646 SDS-PAGE and immunoblotting.

647

648 **Mass spectrometry**.

649 Cells were grown in YPD until OD of 0.75 and added 0.5 mM auxin for
650 40min. 150 ODs of cells were harvested, and membrane fraction was
651 prepared using bead beating as described above. The pelleted
652 membranes were solubilized in 1.2mL in LB supplemented with 1%
653 Triton X-100 and incubated overnight with 75 μL anti-HA beads
654 (Pierce TM). Beads were washed 3 times with LB +1% Triton X-100
655 and bound proteins eluted with 100 μL SB buffer and 95% was
656 separated by SDS-PAGE and Coomassie-stained. In parallel
657 immunoblotting was performed in 5% of the same sample against HA
658 epitope. The fragments bands were excised from the Coomassie-
659 stained gel and subjected to in-gel trypsin digestion as previously
660 described (Shevchenko et al., 2006). After digestion, peptides were
661 separated by nano-flow reversed-phase liquid chromatography
662 coupled to Q Exactive Hybrid Quadrupole-Orbitrap mass spectrometer
663 (Thermo Fisher Scientific). Peptides were loaded on a C18 PepMap100
664 pre-column (inner diameter 300μm×5mm, 3 μm C18 beads; Thermo
665 Fisher Scientific) and separated on a 50 cm reversed-phase C18

666 column (inner diameter 75 μm, 2 μm C18 beads) using a linear
667 gradient from 10 to 35% of B for 30 min at a flow rate of 200 nL/min
668 (A: 0.1% formic acid, B: 0.1% formic acid in acetonitrile). All data were
669 acquired in a data-dependent mode, automatically switching from MS
670 to collision-induced dissociation MS/MS on the top 10 most abundant
671 ions with a precursor scan range of 350–2000m/z. MS spectra were
672 acquired at a resolution of 70 000 and MS/MS scans at 17 500.
673 Dynamic exclusion was enabled with an exclusion duration of 5 s and
674 charge exclusion was applied to unassigned, and mono-charged ions.
675 Raw data files were processed for protein identification using
676 MaxQuant, version 1.6.3.4 (Tyanova et al., 2016). The MS/MS spectra
677 were searched against the relevant Uniprot proteome database;
678 precursor mass tolerance was set to 20 ppm and MS/MS tolerance to
679 0.05 Da. Enzyme specificity was set to trypsin with a maximum of two
680 missed cleavages. False discovery rate for protein and peptide spectral
681 matches was set at 0.01.

682

683 **Acknowledgements**

684 We thank M. Glickman, F. Wilfing and D Wolf for reagents, members of
685 the Carvalho lab for discussions and M Freeman, L. Krshnan, T.
686 Rapoport, J. Robson-Tull and M. Weijer for comments on the
687 manuscript. Proteomics experiments were performed at Advanced
688 proteomics facility, Department of Biochemistry, University of Oxford.
689 P. Carvalho was supported by an investigator award from The
690 Wellcome Trust (202642/Z/16/Z).

691

692

693 **References**

694 Arkowitz, R.A., Joly, J.C., and Wickner, W. (1993). Translocation can
695 drive the unfolding of a preprotein domain. EMBO J. *12*, 243–253.

696 Baek, G.H., Kim, I., and Rao, H. (2011). The Cdc48 ATPase modulates
697 the interaction between two proteolytic factors Ufd2 and Rad23. Proc.
698 Natl. Acad. Sci. USA *108*, 13558–13563.

699 Baldridge, R.D., and Rapoport, T.A. (2016). Autoubiquitination of the
700 hrd1 ligase triggers protein retrotranslocation in ERAD. Cell *166*, 394–
701 407.

702 Bays, N.W., Wilhovsky, S.K., Goradia, A., Hodgkiss-Harlow, K., and
703 Hampton, R.Y. (2001). HRD4/NPL4 is required for the proteasomal
704 processing of ubiquitinated ER proteins. Mol. Biol. Cell *12*, 4114–4128.

705 Ben-Shem, A., Fass, D., and Bibi, E. (2007). Structural basis for
706 intramembrane proteolysis by rhomboid serine proteases. Proc. Natl.
707 Acad. Sci. USA *104*, 462–466.

708 Bhamidipati, A., Denic, V., Quan, E.M., and Weissman, J.S. (2005).
709 Exploration of the topological requirements of ERAD identifies Yos9p
710 as a lectin sensor of misfolded glycoproteins in the ER lumen. Mol. Cell
711 *19*, 741–751.

712 Bhattacharya, A., and Qi, L. (2019). ER-associated degradation in health
713 and disease - from substrate to organism. J. Cell Sci. *132*.

714 Bodnar, N.O., and Rapoport, T.A. (2017). Molecular mechanism of
715 substrate processing by the cdc48 atpase complex. Cell *169*, 722–
716 735.e9.

717 Carvalho, P., Goder, V., and Rapoport, T.A. (2006). Distinct ubiquitin-
718 ligase complexes define convergent pathways for the degradation of
719 ER proteins. Cell *126*, 361–373.

720 Carvalho, P., Stanley, A.M., and Rapoport, T.A. (2010).
721 Retrotranslocation of a misfolded luminal ER protein by the ubiquitin-
722 ligase Hrd1p. Cell *143*, 579–591.

723 Christianson, J.C., and Ye, Y. (2014). Cleaning up in the endoplasmic
724 reticulum: ubiquitin in charge. Nat. Struct. Mol. Biol. *21*, 325–335.

725 Coyaud, E., Mis, M., Laurent, E.M.N., Dunham, W.H., Couzens, A.L.,
726 Robitaille, M., Gingras, A.-C., Angers, S., and Raught, B. (2015). BioID-
727 based Identification of Skp Cullin F-box (SCF)β-TrCP1/2 E3 Ligase
728 Substrates. Mol. Cell Proteomics *14*, 1781–1795.

729 Denic, V., Quan, E.M., and Weissman, J.S. (2006). A luminal surveillance
730 complex that selects misfolded glycoproteins for ER-associated
731 degradation. Cell *126*, 349–359.

732 Eilers, M., and Schatz, G. (1986). Binding of a specific ligand inhibits
733 import of a purified precursor protein into mitochondria. Nature *322*,
734 228–232.

735 Fink, G.R., and Guthrie, C. (1991). Guide to yeast genetics and molecular
736 biology.

737 Freeman, M. (2014). The rhomboid-like superfamily: molecular
738 mechanisms and biological roles. Annu. Rev. Cell Dev. Biol. *30*, 235–
739 254.

740 Gambill, B.D., Voos, W., Kang, P.J., Miao, B., Langer, T., Craig, E.A., and
741 Pfanner, N. (1993). A dual role for mitochondrial heat shock protein 70
742 in membrane translocation of preproteins. J. Cell Biol. *123*, 109–117.

743 Goder, V., Carvalho, P., and Rapoport, T.A. (2008). The ER-associated
744 degradation component Der1p and its homolog Dfm1p are contained
745 in complexes with distinct cofactors of the ATPase Cdc48p. FEBS Lett.
746 *582*, 1575–1580.

747 Greenblatt, E.J., Olzmann, J.A., and Kopito, R.R. (2011). Derlin-1 is a
748 rhomboid pseudoprotease required for the dislocation of mutant α-1
749 antitrypsin from the endoplasmic reticulum. Nat. Struct. Mol. Biol. *18*,
750 1147–1152.

751 Hitchcock, A.L., Auld, K., Gygi, S.P., and Silver, P.A. (2003). A subset of
752 membrane-associated proteins is ubiquitinated in response to
753 mutations in the endoplasmic reticulum degradation machinery. Proc.
754 Natl. Acad. Sci. USA *100*, 12735–12740.

755 Hoppe, T., Matuschewski, K., Rape, M., Schlenker, S., Ulrich, H.D., and
756 Jentsch, S. (2000). Activation of a membrane-bound transcription
757 factor by regulated ubiquitin/proteasome-dependent processing. Cell
758 *102*, 577–586.

759 Jarosch, E., Taxis, C., Volkwein, C., Bordallo, J., Finley, D., Wolf, D.H., and
760 Sommer, T. (2002). Protein dislocation from the ER requires
761 polyubiquitination and the AAA-ATPase Cdc48. Nat. Cell Biol. *4*, 134–
762 139.

763 Jentsch, S., and Rumpf, S. (2007). Cdc48 (p97): a "molecular gearbox" in
764 the ubiquitin pathway? Trends Biochem. Sci. *32*, 6–11.

765 Knop, M., Finger, A., Braun, T., Hellmuth, K., and Wolf, D.H. (1996).
766 Der1, a novel protein specifically required for endoplasmic reticulum
767 degradation in yeast. EMBO J. *15*, 753–763.

768 Koch, B.A., Jin, H., Tomko, R.J., and Yu, H.-G. (2019). The anaphase-
769 promoting complex regulates the degradation of the inner nuclear
770 membrane protein Mps3. J. Cell Biol. *218*, 839–854.

771 Kohlmann, S., Schäfer, A., and Wolf, D.H. (2008). Ubiquitin ligase Hul5
772 is required for fragment-specific substrate degradation in endoplasmic
773 reticulum-associated degradation. J. Biol. Chem. *283*, 16374–16383.

774 Kreutzberger, A.J.B., and Urban, S. (2018). Single-Molecule Analyses
775 Reveal Rhomboid Proteins Are Strict and Functional Monomers
776 in the Membrane. Biophys. J. *115*, 1755–1761.

777 Laughery, M.F., Hunter, T., Brown, A., Hoopes, J., Ostbye, T., Shumaker,
778 T., and Wyrick, J.J. (2015). New vectors for simple and streamlined
779 CRISPR-Cas9 genome editing in Saccharomyces cerevisiae. Yeast *32*,
780 711–720.

781 Lemberg, M.K., and Freeman, M. (2007). Cutting proteins within lipid
782 bilayers: rhomboid structure and mechanism. Mol. Cell *28*, 930–940.

783 Lemberg, M.K., Menendez, J., Misik, A., Garcia, M., Koth, C.M., and
784 Freeman, M. (2005). Mechanism of intramembrane proteolysis
785 investigated with purified rhomboid proteases. EMBO J. *24*, 464–472.

786 Lilley, B.N., and Ploegh, H.L. (2004). A membrane protein required for
787 dislocation of misfolded proteins from the ER. Nature *429*, 834–840.

788 Longtine, M.S., McKenzie, A., Demarini, D.J., Shah, N.G., Wach, A.,
789 Brachat, A., Philippsen, P., and Pringle, J.R. (1998). Additional modules
790 for versatile and economical PCR-based gene deletion and modification
791 in Saccharomyces cerevisiae. Yeast *14*, 953–961.

792 Medicherla, B., Kostova, Z., Schaefer, A., and Wolf, D.H. (2004). A
793 genomic screen identifies Dsk2p and Rad23p as essential components
794 of ER-associated degradation. EMBO Rep. *5*, 692–697.

795 Mehnert, M., Sommer, T., and Jarosch, E. (2014). Der1 promotes
796 movement of misfolded proteins through the endoplasmic reticulum
797 membrane. Nat. Cell Biol. *16*, 77–86.

798 Morawska, M., and Ulrich, H.D. (2013). An expanded tool kit for the
799 auxin-inducible degron system in budding yeast. Yeast *30*, 341–351.

800 Natarajan, N., Foresti, O., Wendrich, K., Stein, A., and Carvalho, P.
801 (2020). Quality control of protein complex assembly by a
802 transmembrane recognition factor. Mol. Cell *77*, 108–119.e9.

803 Neal, S., Jaeger, P.A., Duttke, S.H., Benner, C., K Glass, C., Ideker, T., and
804 Hampton, R.Y. (2018). The dfm1 derlin is required for ERAD
805 retrotranslocation of integral membrane proteins. Mol. Cell *69*, 306–
806 320.e4.

807 Needham, P.G., Guerriero, C.J., and Brodsky, J.L. (2019). Chaperoning
808 Endoplasmic Reticulum-Associated Degradation (ERAD) and Protein
809 Conformational Diseases. Cold Spring Harb. Perspect. Biol. *11*.

810 Neuber, O., Jarosch, E., Volkwein, C., Walter, J., and Sommer, T. (2005).
811 Ubx2 links the Cdc48 complex to ER-associated protein degradation.
812 Nat. Cell Biol. *7*, 993–998.

813 Nishimura, K., Fukagawa, T., Takisawa, H., Kakimoto, T., and Kanemaki,
814 M. (2009). An auxin-based degron system for the rapid depletion of
815 proteins in nonplant cells. Nat. Methods *6*, 917–922.

816 Oda, Y., Okada, T., Yoshida, H., Kaufman, R.J., Nagata, K., and Mori, K.
817 (2006). Derlin-2 and Derlin-3 are regulated by the mammalian

818 unfolded protein response and are required for ER-associated
819 degradation. J. Cell Biol. *172*, 383–393.

820 Richly, H., Rape, M., Braun, S., Rumpf, S., Hoege, C., and Jentsch, S.
821 (2005). A series of ubiquitin binding factors connects CDC48/p97 to
822 substrate multiubiquitylation and proteasomal targeting. Cell *120*, 73–
823 84.

824 Ruggiano, A., Foresti, O., and Carvalho, P. (2014). ER-associated
825 degradation: protein quality control and beyond. J. Cell Biol. *204*, 869–
826 879.

827 Ruggiano, A., Mora, G., Buxó, L., and Carvalho, P. (2016). Spatial control
828 of lipid droplet proteins by the ERAD ubiquitin ligase Doa10. EMBO J.
829 *35*, 1644–1655.

830 Sato, B.K., and Hampton, R.Y. (2006). Yeast Derlin Dfm1 interacts with
831 Cdc48 and functions in ER homeostasis. Yeast *23*, 1053–1064.

832 Schoebel, S., Mi, W., Stein, A., Ovchinnikov, S., Pavlovicz, R., DiMaio, F.,
833 Baker, D., Chambers, M.G., Su, H., Li, D., et al. (2017). Cryo-EM structure
834 of the protein-conducting ERAD channel Hrd1 in complex with Hrd3.
835 Nature *548*, 352–355.

836 Schuberth, C., and Buchberger, A. (2005). Membrane-bound Ubx2
837 recruits Cdc48 to ubiquitin ligases and their substrates to ensure
838 efficient ER-associated protein degradation. Nat. Cell Biol. *7*, 999–1006.

839 Shevchenko, A., Tomas, H., Havlis, J., Olsen, J.V., and Mann, M. (2006).
840 In-gel digestion for mass spectrometric characterization of proteins
841 and proteomes. Nat. Protoc. *1*, 2856–2860.

842 Shi, J., Hu, X., Guo, Y., Wang, L., Ji, J., Li, J., and Zhang, Z.-R. (2019). A
843 technique for delineating the unfolding requirements for substrate

844 entry into retrotranslocons during endoplasmic reticulum-associated
845 degradation. J. Biol. Chem. *294*, 20084–20096.

846 Stein, A., Ruggiano, A., Carvalho, P., and Rapoport, T.A. (2014). Key
847 steps in ERAD of luminal ER proteins reconstituted with purified
848 components. Cell *158*, 1375–1388.

849 Stolz, A., Schweizer, R.S., Schäfer, A., and Wolf, D.H. (2010). Dfm1 forms
850 distinct complexes with Cdc48 and the ER ubiquitin ligases and is
851 required for ERAD. Traffic *11*, 1363–1369.

852 Tirosh, B., Furman, M.H., Tortorella, D., and Ploegh, H.L. (2003). Protein
853 unfolding is not a prerequisite for endoplasmic reticulum-to-cytosol
854 dislocation. J. Biol. Chem. *278*, 6664–6672.

855 Tsuchiya, H., Ohtake, F., Arai, N., Kaiho, A., Yasuda, S., Tanaka, K., and
856 Saeki, Y. (2017). In Vivo Ubiquitin Linkage-type Analysis Reveals that
857 the Cdc48-Rad23/Dsk2 Axis Contributes to K48-Linked Chain
858 Specificity of the Proteasome. Mol. Cell *66*, 488–502.e7.

859 Tyanova, S., Temu, T., and Cox, J. (2016). The MaxQuant computational
860 platform for mass spectrometry-based shotgun proteomics. Nat.
861 Protoc. *11*, 2301–2319.

862 Vasic, V., Denkert, N., Schmidt, C.C., Riedel, D., Stein, A., and Meinecke,
863 M. (2020). Hrd1 forms the retrotranslocation pore regulated by auto-
864 ubiquitination and binding of misfolded proteins. Nat. Cell Biol. *22*,
865 274–281.

866 Wang, Y., Zhang, Y., and Ha, Y. (2006). Crystal structure of a rhomboid
867 family intramembrane protease. Nature *444*, 179–180.

868 Wolf, D.H., and Stolz, A. (2012). The Cdc48 machine in endoplasmic
869 reticulum associated protein degradation. Biochim. Biophys. Acta *1823*,
870 117–124.

871 Wu, X., and Rapoport, T.A. (2018). Mechanistic insights into ER-
872 associated protein degradation. Curr. Opin. Cell Biol. *53*, 22–28.

873 Wu, X., Siggel, M., Ovchinnikov, S., Mi, W., Svetlov, V., Nudler, E., Liao, M.,
874 Hummer, G., and Rapoport, T.A. (2020). Structural basis of ER-
875 associated protein degradation mediated by the Hrd1 ubiquitin ligase
876 complex. Science *368*.

877 Wu, Z., Yan, N., Feng, L., Oberstein, A., Yan, H., Baker, R.P., Gu, L., Jeffrey,
878 P.D., Urban, S., and Shi, Y. (2006). Structural analysis of a rhomboid
879 family intramembrane protease reveals a gating mechanism for
880 substrate entry. Nat. Struct. Mol. Biol. *13*, 1084–1091.

881 Yasuda, S., Tsuchiya, H., Kaiho, A., Guo, Q., Ikeuchi, K., Endo, A., Arai, N.,
882 Ohtake, F., Murata, S., Inada, T., et al. (2020). Stress- and ubiquitylation-
883 dependent phase separation of the proteasome. Nature *578*, 296–300.

884 Ye, Y., Meyer, H.H., and Rapoport, T.A. (2001). The AAA ATPase
885 Cdc48/p97 and its partners transport proteins from the ER into the
886 cytosol. Nature *414*, 652–656.

887 Ye, Y., Shibata, Y., Yun, C., Ron, D., and Rapoport, T.A. (2004). A
888 membrane protein complex mediates retro-translocation from the ER
889 lumen into the cytosol. Nature *429*, 841–847.

890

891 **Figure legends**

892 **Figure 1. Inducible Retro-Clogger (iRC), an inducible substrate to**
893 **study protein retrotranslocation.**

894 (A) Scheme of the inducible Retro-Clogger (iRC) substrate. The
895 individual modules that compose the iRC are indicated. Numbers
896 indicate the amino acid borders of each module.

897 (B) iRC is membrane-associated. Crude membrane (M) and soluble (S)
898 fractions from *WT* cells expressing iRC were prepared and analyzed by
899 SDS-PAGE and western blotting using an α-HA antibody. The ER-
900 associated protein Kar2 and the cytosolic phosphoglycerate kinase
901 (Pgk1) proteins were used as controls and detected with α-Kar2 and
902 Pgk1 antibodies, respectively.

903 (C) The iRC adopts a type I topology with the N-terminus in the ER
904 lumen. Whole-cell extracts of *WT* cells expressing iRC were treated
905 with PNGase F and analyzed by SDS–PAGE and western blotting using
906 an α-HA antibody. The non-glycosylated dolichol phosphate mannose
907 synthase (Dpm1) was used as a loading control and detected with the
908 α-Dpm1 antibody

909 (D) Schematic representation of the topology of the iRC chimera and of
910 its auxin-dependent ubiquitination.

911 (E) Time-course analysis of iRC stability in cells expressing AtTir1
912 under the indicated conditions. Auxin (IAA) and cycloheximide (CHX)
913 were added at time 0 and were used at 0.4mM and 125μg/ml,
914 respectively. Note that addition of IAA leads to the appearance of faint
915 high molecular weight smear consistent with iRC ubiquitination (Ub-
916 iRC in Long exposure). There is also the appearance of a faint low

917 molecular doublet in late timepoints after IAA addition (#). Whole-cell
918 extracts were analyzed by SDS–PAGE and western blotting. iRC and
919 AtTir1 were detected with α-HA and α-Myc antibodies, respectively.
920 Dpm1 was used as a loading control and detected with the α-Dpm1
921 antibody. Timepoints are in minutes.

922 (F) Dependence of auxin concentration in iRC degradation. Levels of
923 iRC in *WT* cells expressing AtTir1 were analyzed after 40min
924 incubation with the indicated concentration (in mM) of auxin (IAA).
925 Samples prepared and analyzed as in (E).

926

927 **Figure 2. Complete iRC degradation requires Dfm1 but not other**
928 **ERAD membrane components.**

929 (A) The degradation of iRC analyzed in cells lacking the indicated ERAD
930 components, as in Figure 1 (E).

931 (B) The iRC degradation was analyzed as in (A) in *WT* cells or cells
932 with the indicated deletions. Note that iRC degradation in cells lacking
933 Dfm1 lead to accumulation of a fragment of ~37kDa (*). This fragment
934 is present in substantially higher amounts and is slightly smaller than
935 the one observed cells expressing Dfm1 (#).

936 (C) Schematic representation of the iRC-derived L (long, in blue) and S
937 (short, in red) fragments present in WT and *dfm1Δ* cells, respectively,
938 as detected by mass spectrometry. Detergent extracts prepared from
939 *WT* and *dfm1Δ* cells treated with 0.4mM of auxin were subjected to
940 immunoprecipitation with HA antibodies. Eluted proteins were
941 analyzed by SDS-PAGE followed by Mass Spectrometry.

942 (D) Degradation of iRC and its variant iRC(Pro) with three point
943 mutations that abolish the tight folding of the DHFR domain in *WT* and
944 *dfm1Δ* cells. Degradation of iRC and iRC(Pro) was induced at time 0
945 with 0.4mM auxin. Samples were prepared and analyzed as in (A).

946

947 **Figure 3. Dfm1 is required for the retrotranslocation of DHFR**
948 **folded domain from iRC.**

949 (A) iRC-derived L and S fragments are membrane-associated. Cell
950 extracts (Input) from *WT* and *dfm1Δ* cells were fractionated in crude
951 membranes (Memb.) and soluble (Sup) material. Where indicated, cells
952 were incubated with IAA (0.4mM for 40 minutes). Fractions were
953 analyzed by SDS-PAGE and western blotting using α-HA antibody. The
954 ER membrane protein Asi2 and the cytosolic soluble Pgk1 were used
955 as controls.

956 (B) Glycosylation status of iRC determined by PNGase F digestion.
957 Denaturing extracts from *WT* and *dfm1Δ* cells incubated with IAA
958 (0.4mM for 10 minutes) were prepared. Upon dilution, extracts were
959 treated with PNGase F and analyzed by SDS–PAGE and western
960 blotting using α-HA antibody.

961 (C) Accessibility of iRC and derived fragments to exogenous proteinase
962 K. ER-derived microsomes from untreated or IAA-treated (0.4mM for
963 40 minutes) *WT* and *dfm1Δ* cells were incubated with Proteinase-K
964 (PK) (50μg/mL) in the presence or absence of 1% Triton X-100 (Tx).
965 Samples were analyzed by SDS-PAGE followed by western blotting
966 using α-HA antibody.

967 (D) Accessibility of iRC and derived fragments to the cysteine-
968 modifying reagent Maleimide-PEG^{5000} (Mal-PEG). Native extracts from
969 IAA-treated (0.4mM for 40 minutes) *WT* and *dfm1Δ* cells were
970 incubated with 5 mM of Mal-PEG in the absence or presence of the
971 detergents Triton X-100 (Tx-100) or SDS, as indicated. Reactions were
972 subjected to immunoprecipitation with HA antibody, and bound
973 proteins were analyzed by SDS-PAGE and immunoblotting with an α-
974 HA. Note that iRC-derived fragments contain two cysteines, both in the
975 DHFR domain (C191 and C258). The number of cysteine residues
976 modified with Mal-PEG (0, 1 or 2) are indicated by unpeg, 1xPEG and
977 2xPEG.

978 (E) Diagram representation of the topology adopted by the iRC-derived
979 L and S fragments in *WT* and *dfm1Δ* cells, respectively.

980

981 **Figure 4. Distinct roles of Dfm1 rhomboid-like motif and Cdc48-**
982 **interacting domain in iRC retrotranslocation.**

983 (A) Time-course analysis of iRC degradation in *dfm1Δ* cells with an
984 empty vector (-) or the indicated *DFM1* variants. Expression of Dfm1
985 variants was driven from the inducible GAL promoter upon growth in
986 galactose containing media. Cells were treated with 0.4 mM Auxin and
987 cycloheximide at time 0. Whole-cell extracts were analyzed by SDS–
988 PAGE and western blotting. iRC and Flag-tagged Dfm1 derivatives were
989 detected with α-HA and α-Flag antibodies respectively. Pgk1 was used
990 as loading control and detected with α-Pgk1 antibody

991 (B) Time-course analysis of iRC degradation in *WT* cells with an empty
992 vector (-) or overexpressing the indicated *DFM1* variants. Samples
993 were prepared and analyzed as in (A).

994 (C) Time-course analysis of iRC degradation in cells with the indicated
995 genotype. The Dfm1(1-283)-SBP lacks the SHP-motifs shown to
996 interact with the Cdc48 ATPase. Samples were prepared and analyzed
997 as in (A). On the right, the graph shows the amount of L fragment in
998 Dfm1(1-283)-SBP cells in relation to the *WT* at the 40 minutes time
999 point. At least three independent experiments were quantified. Error
1000 bars indicate the standard error of the mean.

1001

1002 **Figure 5. Dfm1 and the Cdc48 complex partner in the**
1003 **retrotranslocation of a luminal folded domain**

1004 (A) Time-course analysis of iRC degradation in cells with the indicated
1005 genotype at 25°C (left panel) or upon a 60 min shift to 37°C (right
1006 panel). At time 0, cells were treated with 50μM Auxin and
1007 cycloheximide. In these cells, iRC ubiquitination is mediated by OsTir1,
1008 which is functional at 37°C (Nishimura et al., 2009). Whole-cell
1009 extracts were analyzed by SDS–PAGE followed by western blotting
1010 with α-HA antibody. Dpm1 was used as loading control and detected
1011 with α-Dpm1 antibody.

1012 (B) Time course analysis of iRC degradation in cells with the indicated
1013 genotype, upon a 2h30 shift to 37°C. Samples were prepared and
1014 analyzed as in (A).

1015 (C) iRC interacts with Dfm1 and Cdc48 ATPase. Cells with the indicated
1016 genotype were shifted to 37°C for 2h30 followed by a 20min
1017 incubation with auxin (50 μM). Detergent solubilized membranes were
1018 subjected to immunoprecipitation with HA antibody, and associated
1019 proteins were analyzed by SDS-PAGE and western blotting. HA-tagged
1020 iRC was detected with the α-HA antibody. Cdc48, Dfm1 and Dpm1

1021 proteins were detected with indicated antibodies. For the α-Dpm1 blot,
1022 the asterisk indicates the light chain of the antibody used for
1023 immunoprecipitation.

1024

1025 **Figure 6. iRC processing by Cdc48 and degradation require Ufd2**
1026 **and the shuttle factors Rad23/Dsk2.**

1027 (A) Time-course analysis of iRC degradation in cells with the indicated
1028 genotype. Samples were prepared and analyzed as in Figure 1(E).

1029 (B) iRC interaction with Cdc48 ATPase depends on its auxin-dependent
1030 degradation and is impaired in the indicated mutants. Cells with the
1031 indicated genotype were incubated in absence or presence of IAA (20
1032 minutes). Cell extracts were subjected to immunoprecipitation with HA
1033 antibody, and associated proteins were analyzed by SDS-PAGE and
1034 western blotting. HA-tagged iRC was detected with α-HA antibody.
1035 Cdc48 and Rpn8 were detected with anti-Cdc48 and anti-Rpn8
1036 antibodies, respectively. Note that in native extracts the iRC substrate
1037 is labile and L fragment is generated even in absence of Auxin, as
1038 confirmed by analysis of the same samples under denaturing
1039 conditions (see Figure S4).

1040 **Figure 7. An outline of the pathway for iRC degradation.** See
1041 discussion for details.

1042

1043 **Legends to the Supplemental Figures**

1044 **Figure S1. Mass spectrometry analysis of iRC-derived L and S**
1045 **fragments.**

1046 (A) Amino acid sequence of iRC. Underlined in blue and red are the
1047 peptides identified by mass spectrometry for the L and S fragments,
1048 respectively.

1049 (B) The intensity of the peptides from the of L and S fragments in *WT*
1050 and *dfm1Δ* cells, respectively, as determined by mass spectrometry.

1051

1052 **Figure S2. Auxin-independent degradation iRC in cells expressing**
1053 ***Oryza sativa* Tir1 (OsTir1).**

1054 *WT* cells expressing the iRC with and without V5-tagged OsTir1 (V5-
1055 OsTir1) were grown in YPD media in the absence of auxin at the
1056 indicated temperature. Whole cell lysates were analyzed by SDS-PAGE
1057 and immunoblotting with the indicated antibodies. Dpm1 was used as
1058 loading control and detected with α-Dpm1 antibody.

1059

1060 **Figure S3. Mutation of the Cdc48 adaptor Ubx2 does not affect iRC**
1061 **retrotranslocation and degradation.**

1062 The degradation of iRC in cells with the indicated genotype was
1063 analyzed as in Figure 1. In this experiment, iRC was expressed from the
1064 strong constitutive *ADH* promoter resulting in > 10 fold higher steady
1065 state levels of iRC, in comparison to a iRC construct expressed from the
1066 weaker *CPY* promoter, used in the majority of the experiments. The
1067 genetic requirements for iRC turnover of were the same irrespective of
1068 the promoter used. However, when expressed from the strong *ADH*
1069 promoter, the turnover of iRC was slower and resulted in higher
1070 amounts of L and S fragments in WT and *dfm1Δ* cells, respectively. This
1071 is consistent with the retrotranslocation of DHFR being rate-limiting.

1072

1073 **Figure S4. Samples used in Figure 6B analyzed under denaturing**
1074 **conditions.**

1075 Whole cells extracts prepared under denaturing conditions were
1076 analyzed by SDS-PAGE and immunoblotting.

1077

Fonseca & Carvalho- Figure 1

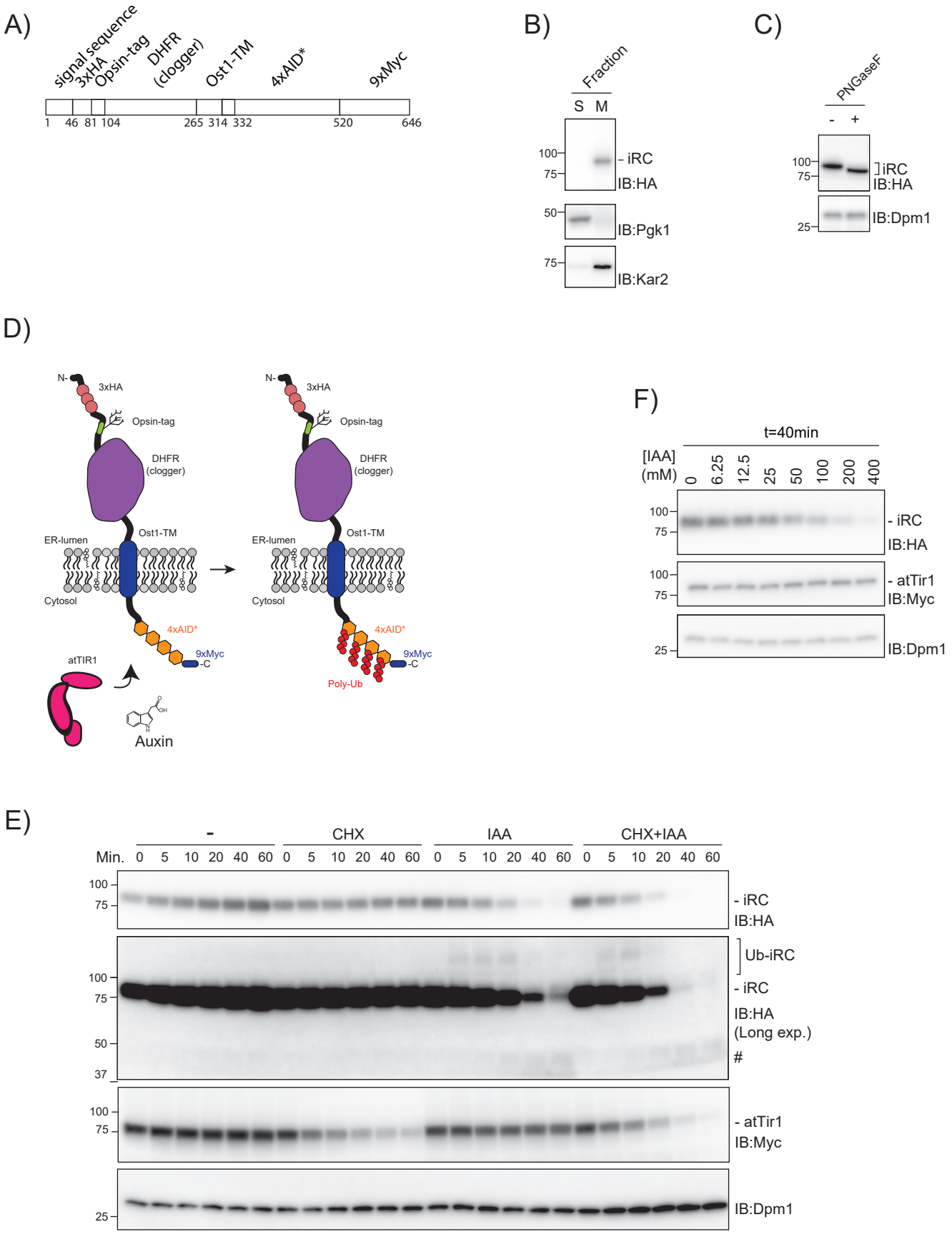

A)

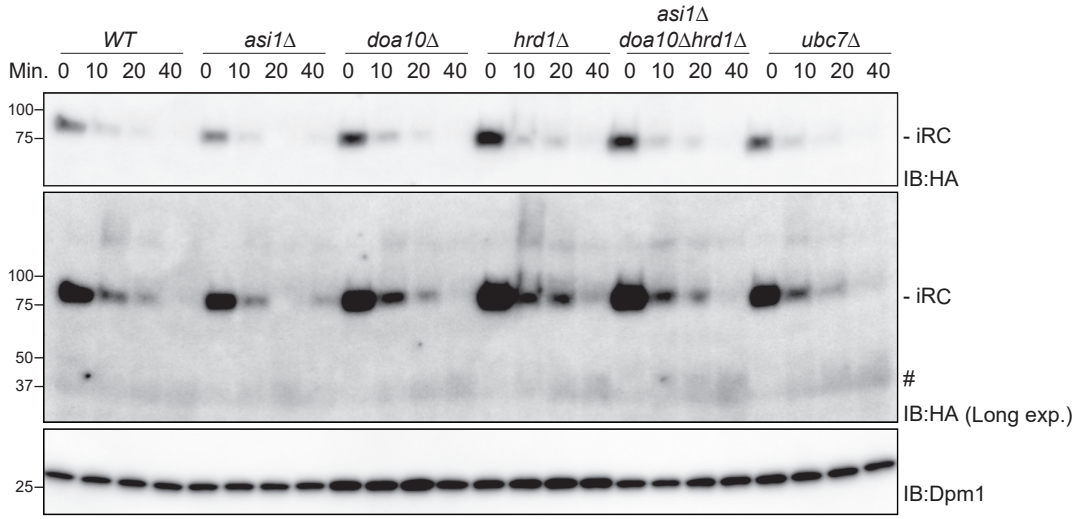

B)

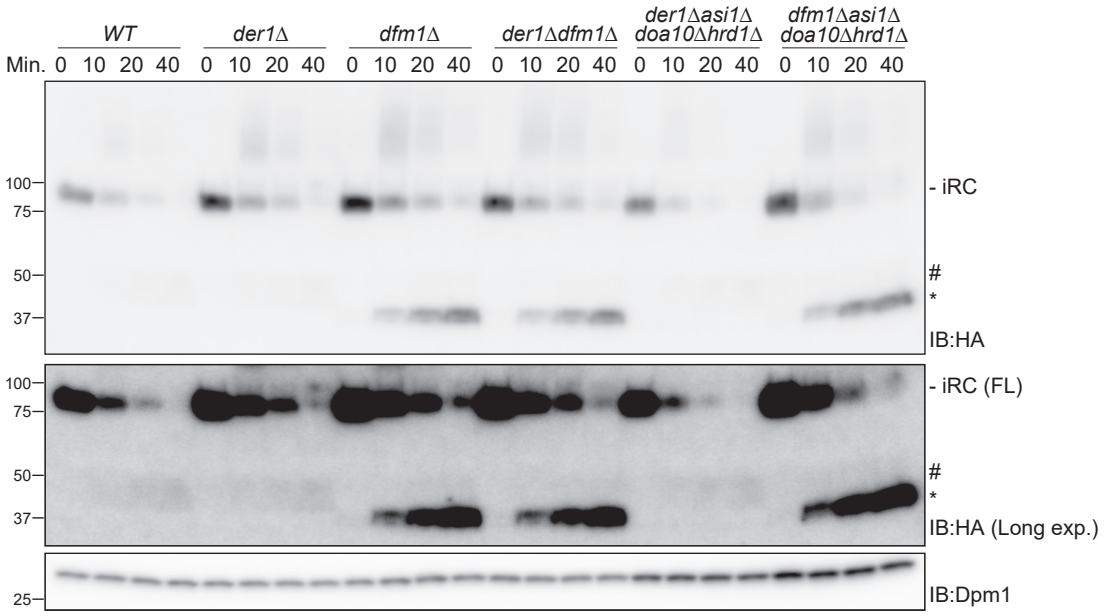

C)

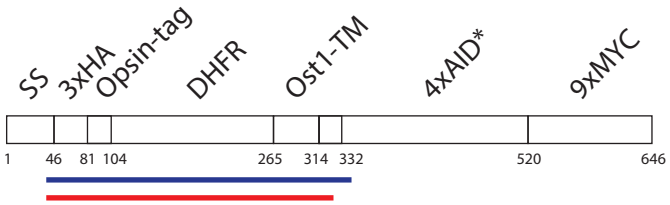

- L fragment (low levels in *WT* cells)
- S fragment (high levels in Δ*dfm1* cells)

D)

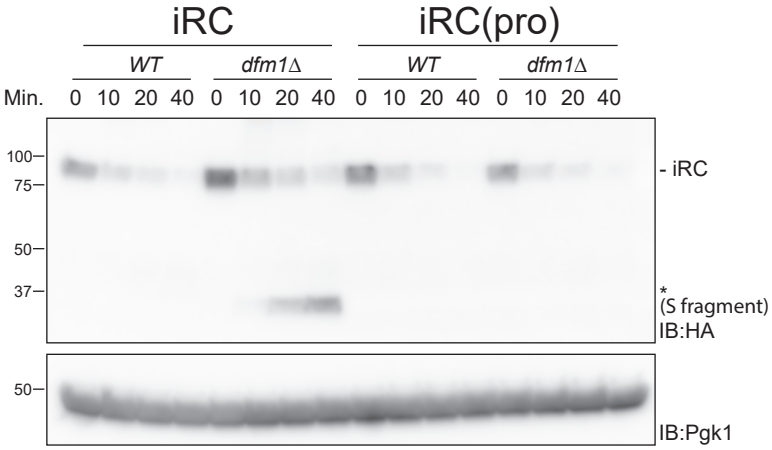

Fonseca & Carvalho- Figure 3

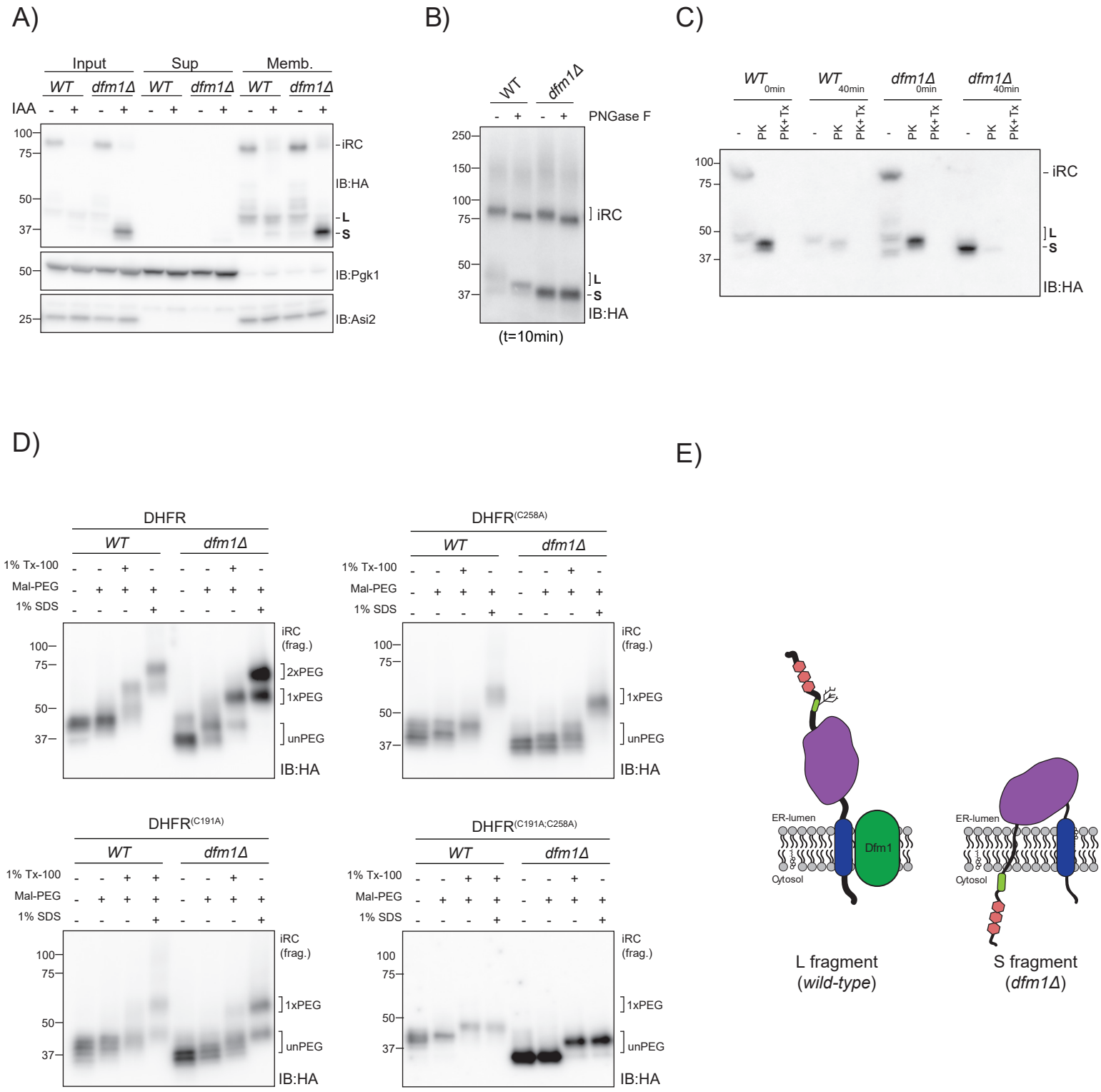

Fonseca & Carvalho- Figure 4

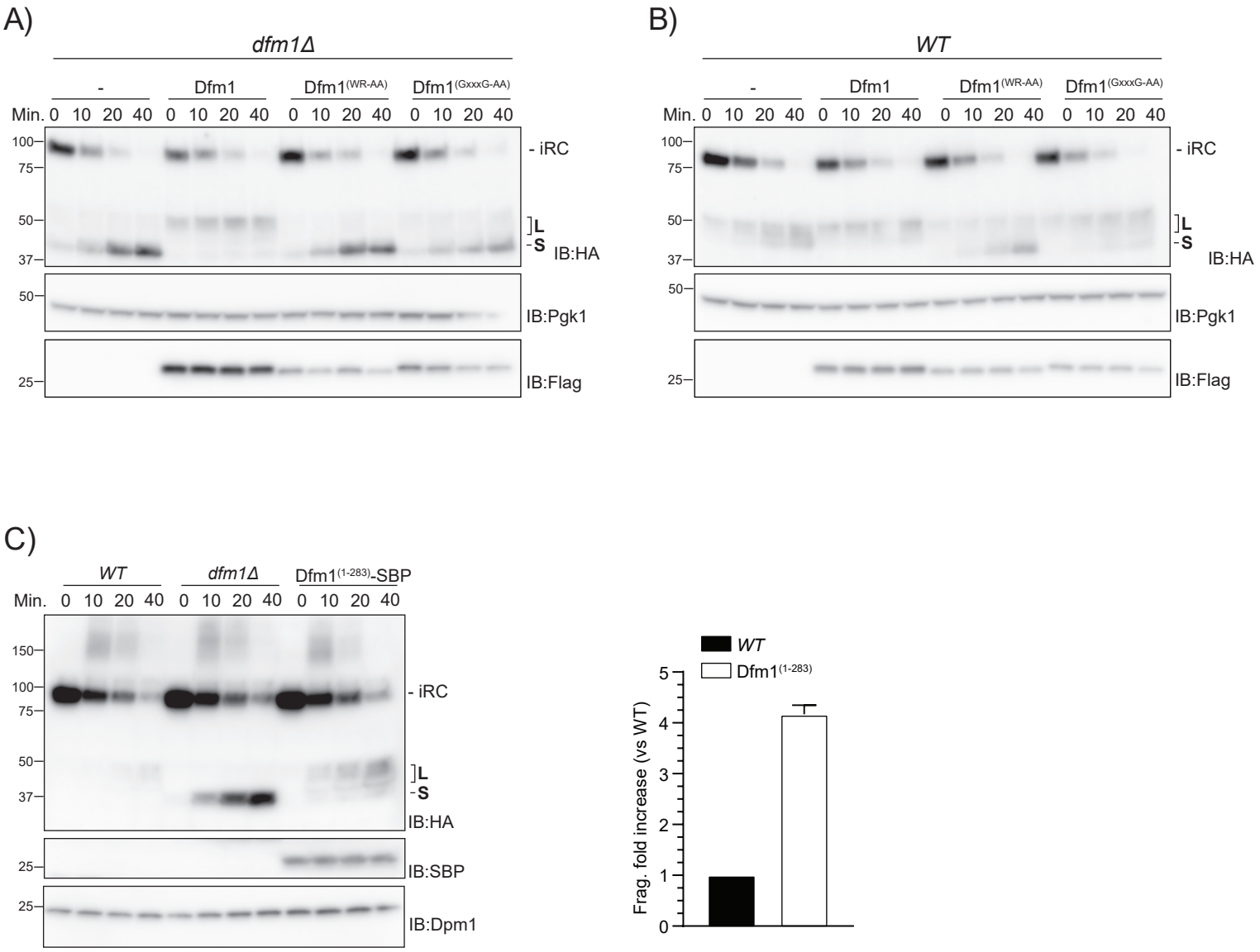

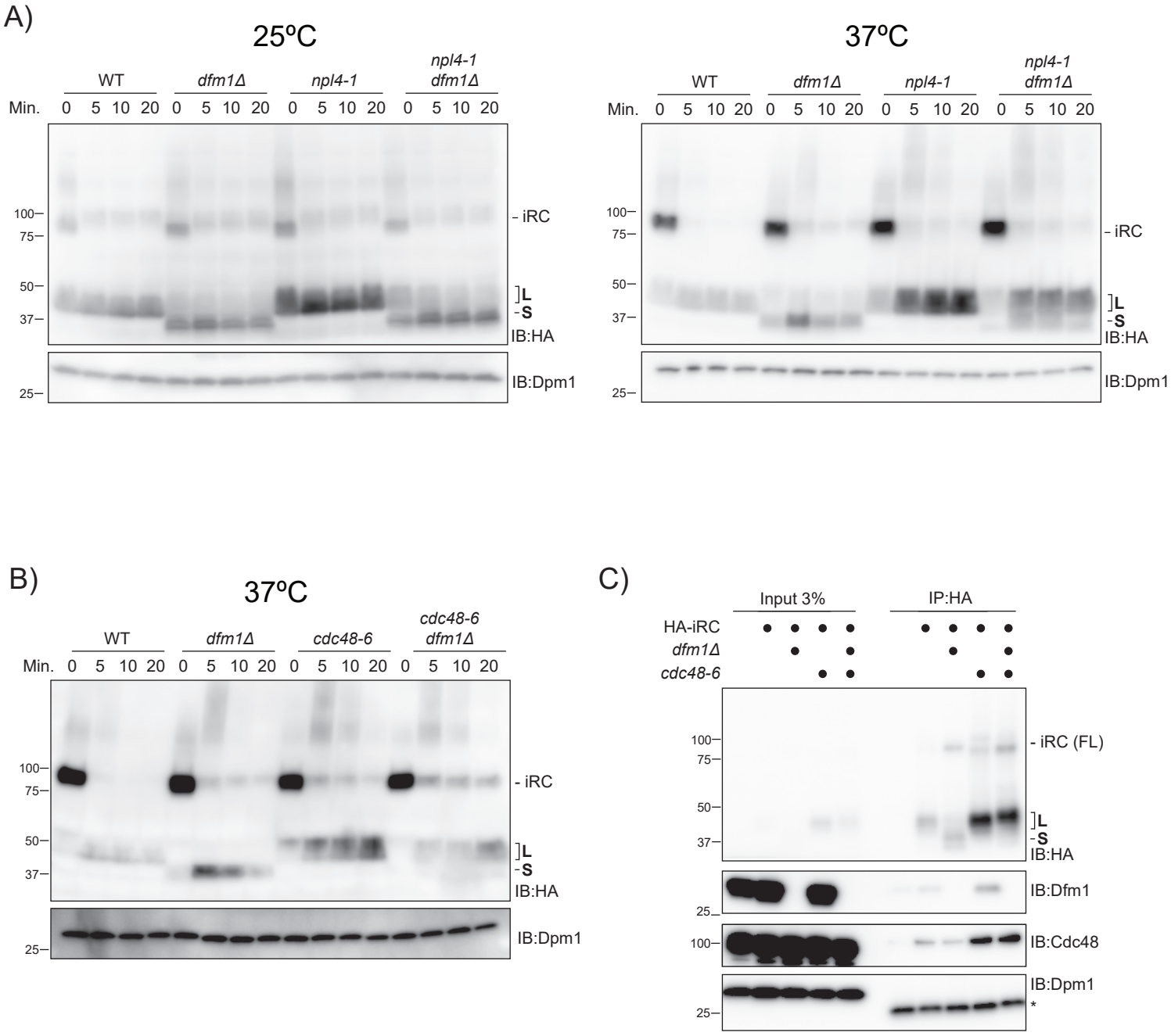
A)
25ºC
37ºC
WT
dfm1Δ
npl4-1
npl4-1 dfm1Δ
Min. 0 5 10 20
100
75
50
37
25
- iRC
L
S
IB:HA
IB:Dpm1
B)
37ºC
cdc48-6
cdc48-6 dfm1Δ
C)
Input 3%
IP:HA
HA-iRC
dfm1Δ
cdc48-6
- iRC (FL)
IB:Dfm1
IB:Cdc48
*

A)

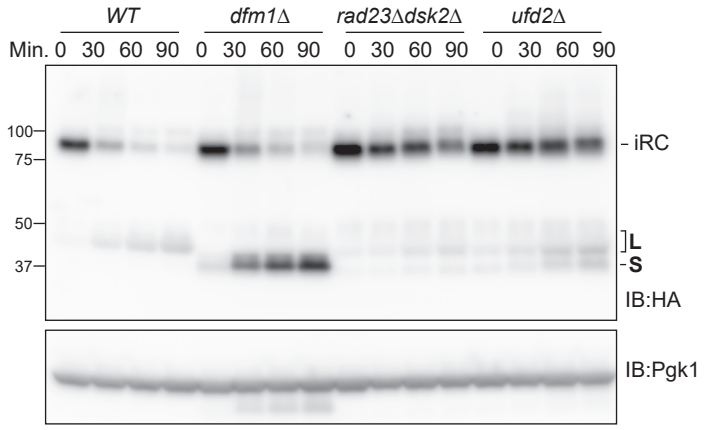
WT
dfm1Δ
rad23Δdsk2Δ
ufd2Δ
Min. 0 30 60 90 0 30 60 90 0 30 60 90 0 30 60 90
100
75
50
37
iRC
L
S
IB:HA
IB:Pgk1

B)

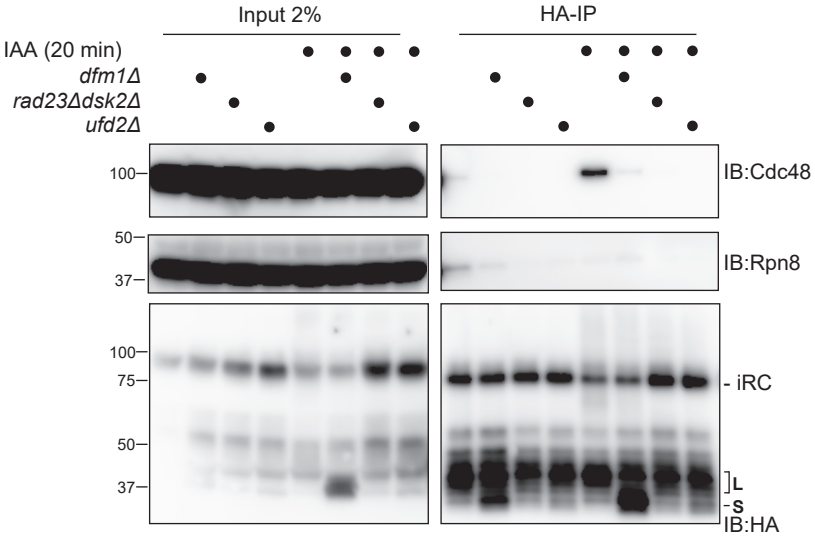
Input 2%
HA-IP
IAA (20 min)
dfm1Δ
rad23Δdsk2Δ
ufd2Δ
100
50
37
IB:Cdc48
IB:Rpn8
100
75
50
37
iRC
L
S
IB:HA

Fonseca & Carvalho- Figure 7

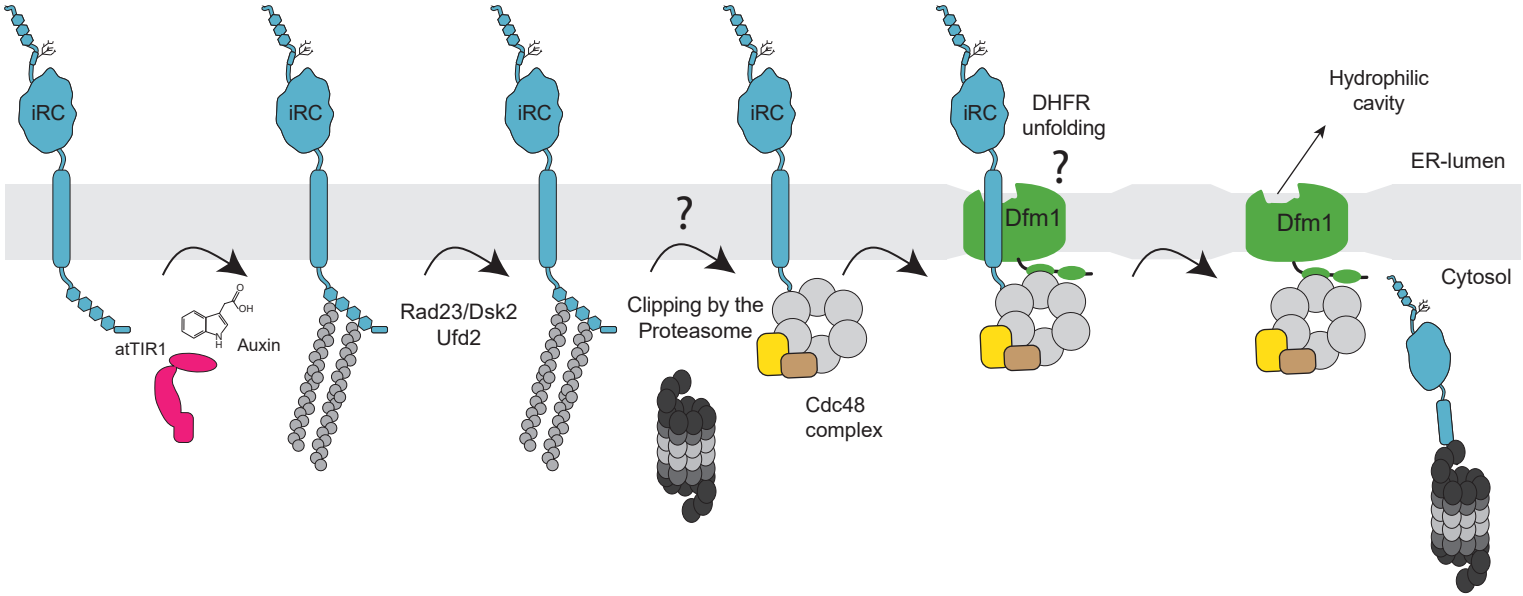

Fonseca & Carvalho- Figure S1

A)

```
        10         20         30         40         50         60
MFFNRLSAGK LLVPLSVVLY ALFVVILPLQ NSFHSSNVLV RGADDVERPA SYPYDVPDYA

        70         80         90        100        110        120
GYPYDVPDYA GSYPYDVPDY AGSSRMNGTE GPNFYGPFSN KTVDGSMISL IAALAVDRVI

       130        140        150        160        170        180
GMENAMPWNL PADLAWFKRN TLNKPVIMGR HTWESIGRPL PGRKNIILSS QPGTDDRVTW

       190        200        210        220        230        240
VKSVDEAIAA CGDVPEIMVI GGGRVYEQFL PKAQKLYLTH IDAEVEGDTH FPDYEPDDWE

       250        260        270        280        290        300
SVFSEFHDAD AQNSHSYCFE ILERRGPSGS GQVLIKYDYP KSSFFKKPLS IACYIFTALM

       310        320        330        340        350        360
GVFVLKTLNM NVTNRTLQVD GAGAGAGAGA GTPKDPAKPP ATAQVVGWPP VRSYRKNVMV

       370        380        390        400        410        420
SCQKSSGGPE AAAFVKVSPG PKDPAKPPAT AQVVGWPPVR SYRKNVMVSC QKSSGGPEAA

       430        440        450        460        470        480
AFVKVSPGPK DPAKPPATAQ VVGWPPVRSY RKNVMVSCQK SSGGPEAAAF VKVSPGPKDP

       490        500        510        520        530        540
AKPPATAQVV GWPPVRSYRK NVMVSCQKSS GGPEAAAFVK VSPGASGEQK LISEEDLNGE

       550        560        570        580        590        600
QKLISEEDLN GEQKLISEED LNGSSRGEQK LISEEDLNGE QKLISEEDLN GEQKLISEED

       610        620        630        640
LNGSSRGEQK ISEEDLNGE QKLISEEDLN GEQKLISEED LNGSTS
```

L-fragment
S-fragment

B)

Sequence	Start position	End position	Peak Intensity WT	Peak Intensity *Δdfm1*
RNTLNKPVIMGR	139	150	1.58E+07	2.05E+07
NTLNKPVIMGR	140	150	2.92E+08	1.85E+09
HTWESIGRPLPGR	151	163	3.21E+07	4.71E+08
HTWESIGRPLPGRK	151	164	1.32E+08	6.25E+08
KNIILSSQPGTDDR	164	177	5.00E+07	2.32E+07
KNIILSSQPGTDDRVTWVK	164	182	5.10E+07	2.56E+08
NIILSSQPGTDDR	165	177	5.56E+08	1.42E+09
NIILSSQPGTDDRVTWVK	165	182	1.91E+09	3.81E+09
SVDEAIAACGDVPEIMVIGGGR	183	204	4.86E+08	8.93E+07
VYEQFLPK	205	212	9.44E+08	2.32E+09
RGPSGSGQVLIK	265	276	1.07E+09	2.75E+09
GPSGSGQVLIK	266	276	0	6.54E+08
TLNMNVTNR	307	315	5.66E+08	1.26E+09
TLQVDGAGAGAGAGAGTPK	316	334	9.81E+08	5.18E+07
TLQVDGAGAGAGAGAGTPKDPAKPPATAQVVGWPPVR	316	352	2.13E+07	0
DPAKPPATAQVVGWPPVR	335	352	5.04E+07	0

Fonseca & Carvalho- Figure S2

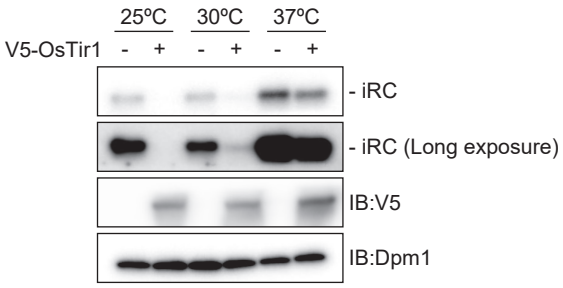

Fonseca & Carvalho- Figure S3

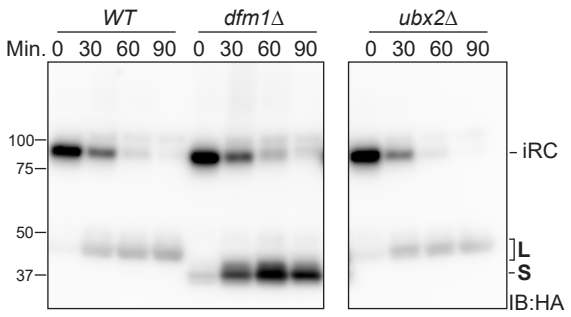
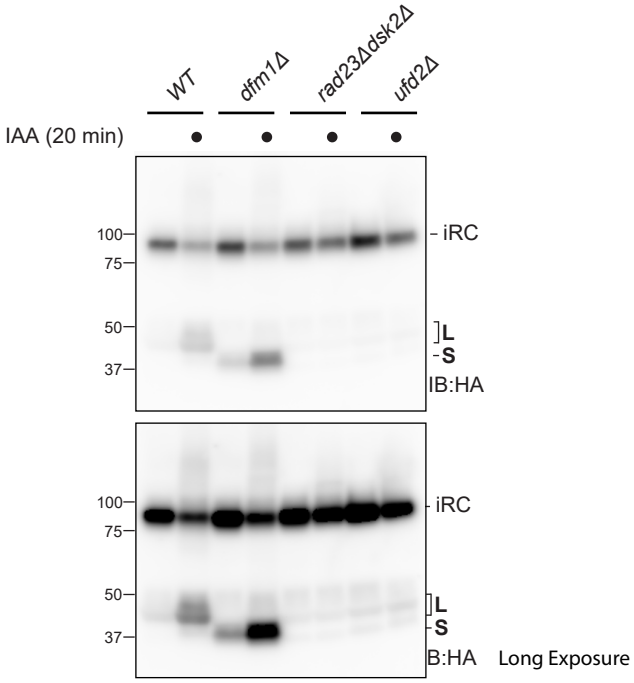
Fonseca & Carvalho- Figure S4